total numbers, the 'classical' CD25$^+$CD4$^+$ T_{reg} cells in aly/aly mice showed no obvious abnormality.

The situation with memory CD4$^+$ cells was very different. Wild-type memory CD25$^-$CD44^{hi}CD4$^+$ T cells functioned like 'typical' antigen-primed T cells: they rapidly generated large amounts of IL-2 after TCR ligation *in vitro* and provided efficient help to naive CD4$^+$ T cells. In contrast, all of the data presented here indicate the conclusion that aly/aly memory CD4$^+$ T cells function as suppressor cells. In every test, both *in vivo* and *in vitro*, elimination of both CD25$^+$ ('typical' T_{reg} cells) and CD25$^-$CD44^{hi}CD4$^+$ memory T cells was required for reversal of the poor proliferative response of aly/aly CD4$^+$ cells. The origin of such 'naturally' occurring CD44^{hi}CD4$^+$ memory cells in either wild-type or NIK-deficient mice is unclear; such cells may arise through contact with various environmental antigens and/or be stimulated by self antigens.

The mechanism of suppression by aly/aly memory CD4$^+$ cells has yet to be resolved. After TCR ligation, suppression correlated with a combination of low IL-2 synthesis and enhanced CD25 expression, which suggests that the cells could function mostly through CD25-mediated consumption of IL-2. That idea fits with the finding that suppression by aly/aly memory CD4$^+$ T cells *in vitro* could be overcome by the addition of exogenous IL-2. However, simple consumption of IL-2 is unlikely to explain the strong inhibitory influence of aly/aly memory CD4$^+$ T cells *in vivo*, which was apparent for both homeostatic proliferation and autoimmune disease induction. By analogy with 'typical' T_{reg} cells, suppression via transforming growth factor-β or IL-10 production could be involved[35–37]; however, at least *in vitro*, production of these cytokines was no higher for aly/aly memory CD4$^+$ T cells than for control memory cells. Hence, resolving the mechanisms of suppression by aly/aly memory CD4$^+$ cells must await further investigation.

Why memory CD4$^+$ cells in aly/aly mice show strong CD25 expression but poor IL-2 synthesis after TCR stimulation is also still unclear. Nevertheless, it is notable that despite enhanced synthesis of CD25, aly/aly memory CD4$^+$ T cells demonstrated very little nuclear translocation of p50, RelA, p52, RelB (as presented here) or c-Rel (data not shown), indicating that CD25 upregulation in aly/aly memory cells involves an NF-κB-independent pathway, such as AP-1 and/or NF-AT[44,45]. Because nuclear translocation of p50-RelA was high in naive aly/aly T cells, the limited translocation of these subunits in memory aly/aly T cells in comparison was unexpected although consistent with the reduced p50 and RelA reported for aly/aly total spleen cells[29]. Based on those preliminary data, poor nuclear translocation of p50 and RelA in memory aly/aly CD4$^+$ cells correlates with reduced synthesis in the cytoplasm, suggesting that p50 and RelA synthesis in memory CD4$^+$ cells is partly controlled by a NIK-dependent pathway. In addition, as in stimulated osteoclast precursors[26], the low amounts of p50 and RelA in aly/aly memory CD4$^+$ cells may be 'held' in the cytoplasm through association with p100; thus, cytoplasmic p100 in aly/aly cells is much higher in memory cells than naive cells.

The hyper-responsiveness of naive aly/aly CD4$^+$ cells was associated with increased synthesis of both IL-2R (CD25) and IL-2, relative to that of wild-type naive cells; detection of an increase in IL-2 synthesis required intracellular staining, presumably because of efficient absorption of extracellular IL-2 by the increased CD25 expressed on the cell surface. Other signs of T cell activation, such as CD69 expression and interferon-γ synthesis, were nearly normal (data not shown), indicating that the hyper-responsiveness was centered on the IL-2–IL-2R axis. As for NF-κB, it is particularly notable that the increased proliferative responses of naive aly/aly CD4$^+$ cells were associated with considerable increases in nuclear translocation of p50 and RelA, apparent in both nuclear extracts and by confocal microscopy. Therefore, this indicates that NIK functions by preventing nuclear translocation of p50 and RelA. The simplest possibility is that NIK regulates autocrine synthesis of p100 through continuous p100-p52 processing, thus allowing nuclear translocation of p52-RelB dimers and transcription of the gene encoding p100 (ref. 26); steady-state production of p100 then keeps p50 and RelA in the cytoplasm. We favor that hypothesis because there was much less p100 in aly/aly naive cells than in control cells; that result was also confirmed by FRET analysis, which showed no apparent association of p100 with p50 or RelA. Hence, we attribute the hyper-responsiveness of aly/aly naive CD4$^+$ cells (as well as *Map3k14*$^{-/-}$ (NIK-deficient) and *Relb*$^{-/-}$ cells) to reduced p100 synthesis, which leads to unregulated nuclear translocation of p50-RelA and enhanced IL-2 and IL-2R synthesis. For *Relb*$^{-/-}$ cells, p100 was also reduced (data not shown), presumably because expression of the gene encoding autocrine p100 is controlled by p52-RelB heterodimers[26].

For naive CD4$^+$ cells from wild-type mice, despite prominent synthesis in the cytoplasm, nuclear translocation of p52-RelB was undetectable within the first 2 d after TCR-CD28–induced activation, indicating no involvement of the nonclassical NF-κB2 pathway. However, by day 3 after TCR ligation, substantial nuclear translocation of p52-RelB was evident, which paralleled a decrease in p50-RelA. That result provides direct support for the hypothesis that NF-κB2–RelB is involved in the later stages of the primary response[46–48], perhaps by 'substituting' for the classical NF-κB1 pathway. One point to emphasize here is that nuclear translocation of NF-κB2–RelB presumably has only a positive effect on gene transcription and thus cannot account for the regulatory effect of NIK on TCR responsiveness. As mentioned above, we envisage that NIK acts as a 'brake' for the NF-κB1 pathway simply by maintaining unprocessed p100 in the cytoplasm, thereby impeding entry of p50-RelA into the nucleus.

In summary, our data here have shown that the T cell defects reported for NIK-deficient mice[13] and *Relb*$^{-/-}$ mice[20] reflect a dominant form of immunoregulation in which otherwise hyper-responsive NIK-deficient naive T cells are suppressed by a subset of NIK-deficient CD25$^-$ memory T cells. Only when the suppressor cells are eliminated is the cell-intrinsic phenotype of NIK-deficiency demonstrated. At face value, these results may seem at odds with the observation that aly/aly mice develop multiorgan autoimmune disease. That syndrome, associated with a reduction in classic CD25$^+$ T_{reg} cells, may be triggered by poor negative selection in the thymus because of reduced expression of various self antigens in the thymic medulla[30]. Given such a self-tolerance defect, it is unexpected that autoimmune disease in aly/aly mice is relatively mild, which suggests that the 'nontolerant' T cells in these mice are generally very well controlled, perhaps by the inhibitory memory subset we have described here. The fulminating autoimmune disease seen when purified naive aly/aly CD4$^+$ cells were transferred adoptively is consistent with that idea.

METHODS

Mice. B6 and 129 mice were obtained from the Jackson Laboratory. *Map3k14*$^{-/-}$ (NIK-deficient), *Map3k14*$^{aly/aly}$ (aly/aly) and *Relb*$^{-/-}$ mice were provided by R. Ulevitch (The Scripps Research Institute, La Jolla, California) and M. Kronenberg (La Jolla Institute for Allergy and Immunology, San Diego, California), and OT-II mice[49] (C57BL/6-Tg(TcraTcrb)425Cbn/J) were obtained from S. Webb (The Scripps Research Institute, La Jolla, California); aly/aly OT-II mice were generated by crossing of aly/aly mice with OT-II mice. *Rag2*$^{-/-}$ mice were obtained from Taconic. All mice were maintained in specific pathogen–free conditions in our animal facility and the experiments were approved by an animal ethics board of The Scripps Research Institute (La Jolla, California) or Tokushima University (Tokushima, Japan).

Antibodies. Antibodies specific for p50 (C-19, NLS and D-17), p52 (K-27 and C-5), RelA (A-20, C-20 and F-6), RelB (C-19), c-Rel, histone and glyceraldehyde phosphate dehydrogenase were purchased from Santa Cruz Biotechnology and were used for immunoprecipitation, immunoblot analysis, EMSA and confocal microscopy.

Cell purification. For purification of CD4$^+$ subsets, lymph node or spleen cells were treated for 45 min at 37 °C with cytotoxic mAbs specific for CD8 (3.168.8) and CD24 (J11D) plus guinea pig complement (Rockland)[50]. After being washed, CD25$^+$CD4$^+$ T cells, NK1.1$^+$ T cells and cells positive for major histocompatibility complex class II first underwent depletion by negative selection with DynaBeads (Dynal). Samples were enriched for CD44^{lo} and CD44^{hi} cells by negative selection with anti-CD44 (IM7) or anti-CD62L (Mel-14) and were positively 'panned' with anti-CD4 (RL172). In addition, samples were enriched for CD44^{lo}, CD44^{int} and CD44^{hi} CD4$^+$ and CD25$^+$CD4$^+$ T cells by cell sorting with a FACSvantage (Becton Dickinson).

Culture conditions. Cells were cultured in 0.2 ml of RPMI medium supplemented with 50 μM 2-mercaptoethanol, L-glutamine and 10% FCS in 96-well tissue culture plates coated with mAbs specific for TCRβ (H57-597) and CD28 (37.51; eBiosciences).

Flow cytometry. A FACSsort (Becton Dickinson) was used for flow cytometry and data were analyzed with FlowJo FACS Analysis software (Tree Star). Analysis of cell division with CFSE (Molecular Probes)[42], intracellular cytokine production (IL-2) with a BD Cytofix/Cytoperm kit (BD Biosciences)[51] and intracellular Foxp3 expression with an Intracellular Foxp3 Detection Kit (eBioscience) was done according to the manufacturers' instructions.

Proliferation assay. Cell proliferation was evaluated by [^{3}H]thymidine incorporation or by counting of divisions by CFSE dilution of labeled cells. In most experiments, 5×10^4 enriched CD4$^+$ T cells were stimulated for 24–72 h with plate-bound mAbs to TCR (0.1-1 μg/ml) and CD28 (20 μg/ml). OT-II T cells (0.625×10^4 to 5×10^4 cells/well) were cultured together with irradiated (3,000 cGy) Thy-1.2$^+$-depleted syngeneic spleen cell samples (5×10^5 cells) and were stimulated with OVA peptide, amino acids 323–339 (Sigma Genosys). Stimulated cells were then pulsed with 0.5 μCi [^{3}H]thymidine per well for the last 8 h of culture. For CFSE labeling, purified CD4$^+$ T cells were resuspended with 0.1% BSA in PBS at a density of 5×10^6 cells/ml and were labeled for 10 min at 37 °C with 0.3 μM CFSE. CFSE-labeled cells were 'quenched' with PBS containing 5% FCS and were washed twice. Cell division at 48–72 h was analyzed by flow cytometry.

EMSA. Nuclear extracts of stimulated CD4$^+$ T cells were prepared as described[52]. Cells were washed twice with PBS and were resuspended in 100 μl ice-cold lysis buffer, were vortexed and were centrifuged for 5 min at 5,000*g*. Nuclear pellets were resuspended in 100 μl extraction buffer containing 20 mM HEPES, 1.5 mM $MgCl_2$, 0.2 mM EDTA, 0.4 mM NaCl, 2.5% glycerol and a mixture of protease inhibitors. After centrifugation for 30 min at 12,000*g*, nuclear extracts (0.5–5 μg) in the supernatant were incubated for 20 min at 25 °C with biotin-labeled κB oligonucleotide probe (5′-AGTTGAGGG GACTTTCCCAGGC-3′) and Oct-1 oligonucleotide probe (5′-TGTCGAATG CAAATCACTAGAA-3′). Protein-DNA complexes were resolved by nondenaturing 4–6% PAGE in 0.5× TBE and were transferred to nylon membranes (Pierce). After crosslinking of transferred DNA to the membranes, biotin-labeled DNA was detected with a LightShift Chemiluminescent EMSA Kit (Pierce) according to the manufacturer's instructions. For supershift assay, NF-κB subunit–specific antibodies were added before the formation of DNA-protein complexes at 25 °C for 15 min.

Immunoprecipitation and immunoblot analysis. Nuclear extracts, cytoplasmic extracts and total cell lysates from CD4$^+$ T cells (2.5–10 μg) were separated by 10% SDS-PAGE and were blotted onto polyvinyldifluoride membranes. Blotted membranes were incubated with antibodies specific for NF-κB subunits, followed by incubation with goat anti-mouse, or donkey anti-rabbit coupled to horseradish peroxidase, and proteins were made visible with the SuperSignal West Pico Chemiluminescent Substrate (Pierce). For immunoprecipitation, purified proteins (10–50 μg) 'captured' with the antibody were incubated with immobilized protein G and were precipitated with a Seize Classic Mammalian Immunoprecipitation Kit (Pierce). Precipitated proteins were analyzed by immunoblot with the NF-κB subunit–specific antibodies described above and a Rabbit IgG TrueBlot set (eBioscience). Positive controls for the detection of NF-κB subunits were confirmed by immunoblot analysis (**Supplementary Fig. 6** online) using Jurkat or A431 cell lysates (BD Transduction Laboratories).

ELISA. The amount of IL-2 and IL-10 proteins in culture supernatants was determined by ELISA. Production of transforming growth factor-β was measured with the DuoSet ELISA Development System (R&D Systems). For this, 96-well flat-bottomed plates were precoated with capture antibodies, and diluted samples or standard recombinant cytokines were added to each well. After plates were washed, biotinylated antibodies were added and then wells were incubated with horseradish peroxidase–labeled, affinity-purified anti-rat immunoglobulin G (IgG). A solution of *o*-phenylendiamine (Sigma) was added to each well as a substrate. The optical density at 490 nm was measured with a microplate reader (Molecular Devices).

Confocal microscopy. Cells were deposited onto poly-L-lysine-coated glass slides, were fixed with 3% paraformaldehyde in PBS, were made permeable for 2 min with 0.2% Triton X-100 in PBS and were preblocked for 1 h with 1% BSA and 2.5% FCS in PBS. Cells were stained for 1 h with 1 μg/ml of the appropriate primary antibodies. After being washed three times with 0.0001% Triton X-100 in PBS, cells were stained for 30 min with secondary Alexa Fluor 488–conjugated donkey anti-mouse or goat anti-rabbit IgG (heavy plus light) and then were washed with PBS. Coverslips were applied with Fluoromount-G (Molecular Probes). Cells were visualized with a BioRad 1024 laser-scanning confocal microscope (BioRad Laboratories). Each optical section was acquired sequentially with 488-nm and 568-nm laser lines to excite Alexa Fluor 488 (green) and Alexa Fluor 568 (red) fluorescence, respectively. Merged images are presented as yellow. For FRET, Zenon Rabbit IgG Labeling Kits or Zenon Mouse IgG Labeling Kits (Molecular Probe) were used to label antibodies with Alexa Fluor 488 as the 'donor dye' or Alexa Fluor 546 as the 'acceptor dye'[53]. Red color indicates that the acceptor dye was activated by the donor dye, as the two dyes were in close proximity.

NF-κB transcription activity assay. The transcriptional activity of NF-κB subunits of the nuclear extracts from naive T cells was analyzed with NF-κB Family Transcription Factor Assay Kit (Chemicon). Nuclear extracts were incubated with biotinylated double-stranded oligonucleotide probe containing the consensus sequence (5′-GGGACTTTCC-3′) for NF-κB on a streptavidin-coated plate. Captured complexes, including active NF-κB protein, were incubated with the primary antibody for NF-κB subunit and horseradish peroxidase–conjugated secondary antibody and tetramethylbenzidine substrate. The absorbance of the samples was measured with a spectrophotometry microplate reader set at 450 nm.

Pulse-chase assay. Purified naive CD4$^+$ T cells from aly/+ and aly/aly mice were cultured for 4 h in methionine-free RPMI 1640 medium (Sigma) supplemented with ^{35}S-labeled methionine (50 μCi/ml) on plates coated with mAbs to TCR and CD28. Purified total extracts were immunoprecipitated with rabbit anti-RelA. Radiolabeled proteins in the immunoprecipitate were resolved by reduced SDS-PAGE; the dried gel was exposed to autoradiography film in a phosphorimaging cassette.

Cell transfer. CFSE-labeled naive or memory CD4$^+$ T cells (5×10^6) from aly/aly, aly/+ or B6.Ly5.1 mice were transferred intravenously into irradiated (700 cGy) B6.PL (Thy-1.1$^+$) or B6 mice. On day 7 after transfer, spleen cells were analyzed to measure homeostatic proliferation via CFSE dilution by flow cytometry. For analysis of *in vivo* antigen-specific T cell responses, 5×10^6 CFSE-labeled naive CD4$^+$ T cells from aly/aly OT-II B6.PL and aly/+ OT-II B6.PL mice were transferred intravenously into B6 mice; OVA peptide of amino acids 323–339 (0–200 μg) was injected intraperitoneally into the mice; 3 d later, proliferation of the donor cells in spleen and lymph node was analyzed by flow cytometry. For induction of autoimmune lesions in aly/aly mice, 5×10^6 enriched total CD4$^+$, CD25$^-$CD4$^+$ or naive CD4$^+$ cells from aly/+ or aly/aly mice were transferred intravenously into *Rag2*$^{-/-}$ mice.

Histological analysis. All organs of *Rag2*$^{-/-}$ mice that had received cell transfer were removed, were fixed with 4% phosphate-buffered formaldehyde, pH 7.2, and were prepared for histological examination. Sections were stained with hematoxylin and eosin. The disease incidence and severity in pancreata and lacrimal glands was determined by the histological score of inflammatory lesions as described[54]. For the inflammatory lesions of lungs, lymphocytes per mm^2 were counted. Histological findings were estimated by three independent, well-trained pathologists 'blinded' to sample identity.

Statistics. Student's *t*-test was used for statistical analyses.

Note: Supplementary information is available on the Nature Immunology website.

ACKNOWLEDGMENTS
We thank B. Marchand for typing the manuscript. Supported by the United States Public Health Service (CA38355, AI21487, AI46710 and AG01743; publication number 17327-IMM from The Scripps Research Institute) and by the Ministry of Education, Science, and Culture of Japan (grants-in-aid for scientific research; 17689049).

COMPETING INTERESTS STATEMENT
The authors declare that they have no competing financial interests.

Published online at http://www.nature.com/natureimmunology/
Reprints and permissions information is available online at http://npg.nature.com/reprintsandpermissions/

1. Ghosh, S., May, M.J. & Kopp, E.B. NF-κB and Rel proteins: evolutionarily conserved mediators of immune responses. *Annu. Rev. Immunol.* **16**, 225–260 (1998).
2. Karin, M. How NF-κB is activated: the role of the IκB kinase (IKK) complex. *Oncogene* **18**, 6867–6874 (1999).
3. Bonizzi, G. & Karin, M. The two NF-κB activation pathways and their role in innate and adaptive immunity. *Trends Immunol.* **25**, 280–288 (2004).
4. Kahn-Perles, B., Lipcey, C., Lecine, P., Olive, D. & Imbert, J. Temporal and subunit-specific modulations of the Rel/NF-κB transcription factors through CD28 costimulation. *J. Biol. Chem.* **272**, 21774–21783 (1997).
5. Sun, Z. *et al.* PKC-theta is required for TCR-induced NF-κB activation in mature but not immature T lymphocytes. *Nature* **404**, 402–407 (2000).
6. Ruland, J. *et al.* Bcl10 is a positive regulator of antigen receptor-induced activation of NF-κB and neural tube closure. *Cell* **104**, 33–42 (2001).
7. Thome, M. & Tschopp, J. TCR-induced NF-κB activation: a crucial role for Carma1, Bcl10 and MALT1. *Trends Immunol.* **24**, 419–424 (2003).
8. Karin, M. & Ben-Neriah, Y. Phosphorylation meets ubiquitination: the control of NF-κB activity. *Annu. Rev. Immunol.* **18**, 621–663 (2000).
9. Pimentel-Muinos, F. *et al.* Regulation of interleukin-2α chain expression and nuclear factor κB activation by protein kinase C in T lymphocytes. Autocrine role of tumor necrosis factor α. *J. Biol. Chem.* **269**, 24424–24429 (1994).
10. Prasad, A.S. *et al.* Zinc enhances the expression of interleukin-2 and interleukin-2 receptors in HUT-78 cells by way of NF-κB activation. *J. Lab. Clin. Med.* **140**, 272–289 (2002).
11. Dejardin, E. *et al.* The lymphotoxin-β receptor induces different patterns of gene expression via two NF-κB pathways. *Immunity* **17**, 525–535 (2002).
12. Matsushima, A. *et al.* Essential role of nuclear factor (NF)-κB-inducing kinase and inhibitor of κB (IκB) kinase α in NF-κB activation through lymphotoxin β receptor, but not through tumor necrosis factor receptor I. *J. Exp. Med.* **193**, 631–636 (2001).
13. Matsumoto, M. *et al.* Essential role of NF-κB-inducing kinase in T cell activation through the TCR/CD3 pathway. *J. Immunol.* **169**, 1151–1158 (2002).
14. Artis, D. *et al.* NF-κB1 is required for optimal CD4+ Th1 cell development and resistance to *Leishmania major*. *J. Immunol.* **170**, 1995–2003 (2003).
15. Erdman, S., Fox, J.G., Dangler, C.A., Feldman, D. & Horwitz, B.H. Typhlocolitis in NF-κB-deficient mice. *J. Immunol.* **166**, 1443–1447 (2001).
16. Hilliard, B., Samoilova, E.B., Liu, T.S., Rostami, A. & Chen, Y. Experimental autoimmune encephalomyelitis in NF-κB-deficient mice:roles of NF-κB in the activation and differentiation of autoreactive T cells. *J. Immunol.* **163**, 2937–2943 (1999).
17. Das, J. *et al.* A critical role for NF-κB in GATA3 expression and T_H2 differentiation in allergic airway inflammation. *Nat. Immunol.* **2**, 45–50 (2001).
18. Beg, A.A., Sha, W.C., Bronson, R.T., Ghosh, S. & Baltimore, D. Embryonic lethality and liver degeneration in mice lacking the RelA component of NF-κB. *Nature* **376**, 167–170 (1995).
19. Burkly, L. *et al.* Expression of RelB is required for the development of thymic medulla and dendritic cells. *Nature* **373**, 531–536 (1995).
20. Weih, F. *et al.* Multiorgan inflammation and hematopoietic abnormalities in mice with a targeted disruption of RelB, a member of the NF-κB/Rel family. *Cell* **80**, 331–340 (1995).
21. Franzoso, G. *et al.* Mice deficient in nuclear factor (NF)-κB/p52 present with defects in humoral responses, germinal center reactions, and splenic microarchitecture. *J. Exp. Med.* **187**, 147–159 (1998).
22. Speirs, K., Lieberman, L., Caamano, J., Hunter, C.A. & Scott, P. Cutting edge: NF-κB2 is a negative regulator of dendritic cell function. *J. Immunol.* **172**, 752–756 (2004).
23. Hilliard, B.A. *et al.* Critical roles of c-Rel in autoimmune inflammation and helper T cell differentiation. *J. Clin. Invest.* **110**, 843–850 (2002).
24. Kontgen, F. *et al.* Mice lacking the c-rel proto-oncogene exhibit defects in lymphocyte proliferation, humoral immunity, and interleukin-2 expression. *Genes Dev.* **9**, 1965–1977 (1995).
25. Shinkura, R. *et al.* Alymphoplasia is caused by a point mutation in the mouse gene encoding Nf-κB-inducing kinase. *Nat. Genet.* **22**, 74–77 (1999).
26. Novack, D.V. *et al.* The IκB function of NF-κB2 p100 controls stimulated osteoclastogenesis. *J. Exp. Med.* **198**, 771–781 (2003).
27. Yin, L. *et al.* Defective lymphotoxin-β receptor-induced NF-κB transcriptional activity in NIK-deficient mice. *Science* **291**, 2162–2165 (2001).
28. Fagarasan, S. *et al.* Alymphoplasia (aly)-type nuclear factor κB-inducing kinase (NIK) causes defects in secondary lymphoid tissue chemokine receptor signaling and homing of peritoneal cells to the gut-associated lymphatic tissue system. *J. Exp. Med.* **191**, 1477–1486 (2000).
29. Yamada, T. *et al.* Abnormal immune function of hemopoietic cells from alymphoplasia (aly) mice, a natural strain with mutant NF-κB-inducing kinase. *J. Immunol.* **165**, 804–812 (2000).
30. Kajiura, F. *et al.* NF-κB-inducing kinase establishes self-tolerance in a thymic stroma-dependent manner. *J. Immunol.* **172**, 2067–2075 (2004).
31. Weih, F. *et al.* Both multiorgan inflammation and myeloid hyperplasia in RelB-deficient mice are T cell dependent. *J. Immunol.* **157**, 3974–3979 (1996).
32. Tsubata, R. *et al.* Autoimmune disease of exocrine organs in immunodeficient alymphoplasia mice: a spontaneous model for Sjogren's syndrome. *Eur. J. Immunol.* **26**, 2742–2748 (1996).
33. Dutton, R.W., Bradley, L.M. & Swain, S.L. T cell memory. *Annu. Rev. Immunol.* **16**, 201–223 (1998).
34. Sprent, J. & Surh, C.D. T cell memory. *Annu. Rev. Immunol.* **20**, 551–579 (2002).
35. Sakaguchi, S. Naturally arising CD4+ regulatory T cells for immunologic self-tolerance and negative control of immune responses. *Annu. Rev. Immunol.* **22**, 531–562 (2004).
36. Fehervari, Z. & Sakaguchi, S. Development and function of CD25+CD4+ regulatory T cells. *Curr. Opin. Immunol.* **16**, 203–208 (2004).
37. Piccirillo, C.A. & Shevach, E.M. Naturally-occurring CD4+CD25+ immunoregulatory T cells: central players in the arena of peripheral tolerance. *Semin. Immunol.* **16**, 81–88 (2004).
38. Khattri, R., Cox, T., Yasayko, S.A. & Ramsdell, F. An essential role for Scurfin in CD4+CD25+ T regulatory cells. *Nat. Immunol.* **4**, 337–342 (2003).
39. Fontenot, J.D., Gavin, M.A. & Rudensky, A.Y. Foxp3 programs the development and function of CD4+CD25+ regulatory T cells. *Nat. Immunol.* **4**, 330–336 (2003).
40. Hori, S., Nomura, T. & Sakaguchi, S. Control of regulatory T cell development by the transcription factor Foxp3. *Science* **299**, 1057–1061 (2003).
41. Lu, L.F., Gondek, D.C., Scott, Z.A. & Noelle, R.J. NF κB-inducing kinase deficiency results in the development of a subset of regulatory T cells, which shows a hyperproliferative activity upon glucocorticoid-induced TNF receptor family-related gene stimulation. *J. Immunol.* **175**, 1651–1657 (2005).
42. Ernst, B., Lee, D-S., Chang, J., Sprent, J. & Surh, C.D. The peptide ligands mediating positive selection in the thymus control T cell survival and homeostatic proliferation in the periphery. *Immunity* **11**, 173–181 (1999).
43. Weil, R. & Israel, A. T-cell-receptor- and B-cell-receptor-mediated activation of NF-κB in lymphocytes. *Curr. Opin. Immunol.* **16**, 374–381 (2004).
44. Kim, H.P. & Leonard, W.J. The basis for TCR-mediated regulation of the IL-2 receptor α chain gene: role of widely separated regulatory elements. *EMBO J.* **21**, 3051–3059 (2002).
45. Schuh, K. *et al.* The interleukin 2 receptor α chain/CD25 promoter is a target for nuclear factor of activated T cells. *J. Exp. Med.* **188**, 1369–1373 (1998).
46. Bren, G.D. *et al.* Transcription of the RelB gene is regulated by NF-κB. *Oncogene* **20**, 7722–7733 (2001).
47. Olashaw, N.E. Inducible activation of RelB in fibroblasts. *J. Biol. Chem.* **271**, 30307–30310 (1996).
48. Ivanov, V.N., Deng, G., Podack, E.R. & Malek, T.R. Pleiotropic effects of Bcl-2 on transcription factors in T cells: potential role of NF-κB p50-p50 for the anti-apoptotic function of Bcl-2. *Int. Immunol.* **7**, 1709–1720 (1995).
49. Robertson, J.M., Jensen, P.E. & Evavold, B.D. DO11.10 and OT-II T cells recognize a C-terminal ovalbumin 323–339 epitope. *J. Immunol.* **164**, 4706–4712 (2000).
50. Kishimoto, H. & Sprent, J. Strong TCR ligation without costimulation causes rapid onset of Fas-dependent apoptosis of naive murine CD4+ T cells. *J. Immunol.* **163**, 1817–1826 (1999).
51. Assenmacher, M., Schmitz, J. & Radbruch, A. Flow cytometric determination of cytokines in activated murine T helper lymphocytes: expression of interleukin-10 in interferon-γ and in interleukin-4-expressing cells. *Eur. J. Immunol.* **24**, 1097–1101 (1994).
52. Grundstrom, S., Anderson, P., Scheipers, P. & Sundstedt, A. Bcl-3 and NFκB p50-p50 homodimers act as transcriptional repressors in tolerant CD4+ T cells. *J. Biol. Chem.* **279**, 8460–8468 (2004).
53. Zal, T. & Gascoigne, N.R. Using live FRET imaging to reveal early protein-protein interactions during T cell activation. *Curr. Opin. Immunol.* **16**, 418–427 (2004).
54. Ishimaru, N. *et al.* Development of autoimmune exocrinopathy resembling Sjogren's syndrome in estrogen-deficient mice of healthy background. *Am. J. Pathol.* **163**, 1481–1490 (2003).

MOLECULAR AND CELLULAR BIOLOGY, Apr. 2006, p. 2924–2935 Vol. 26, No. 8
0270-7306/06/$08.00+0 doi:10.1128/MCB.26.8.2924–2935.2006
Copyright © 2006, American Society for Microbiology. All Rights Reserved.

Novel Role for RbAp48 in Tissue-Specific, Estrogen Deficiency-Dependent Apoptosis in the Exocrine Glands

Naozumi Ishimaru,[1] Rieko Arakaki,[1] Fumie Omotehara,[1] Koichi Yamada,[2] Kenji Mishima,[2] Ichiro Saito,[2] and Yoshio Hayashi[1]*

Department of Oral Molecular Pathology, Institute of Health Biosciences, The University of Tokushima Graduate School, 3 Kuramotocho, Tokushima 770-8504,[1] and Department of Pathology, Tsurumi University School of Dentistry, Tsurumi,[2] Japan

Received 1 August 2005/Returned for modification 31 August 2005/Accepted 20 January 2006

Although tissue-specific apoptosis in the exocrine glands in estrogen-deficient mice may contribute to the development of autoimmune exocrinopathy, the molecular mechanism responsible for tissue-specific apoptosis remains obscure. Here we show that RbAp48 overexpression induces p53-mediated apoptosis in the exocrine glands caused by estrogen deficiency. RbAp48-inducible transfectant results in rapid apoptosis with p53 phosphorylation (Ser9) and α-fodrin cleavage. Reducing the expression of RbAp48 through small interfering RNA inhibits the apoptosis. Prominent RbAp48 expression with apoptosis was observed in the exocrine glands of C57BL/6 ovariectomized (OVX) mice but not in OVX estrogen receptor $\alpha^{-/-}$, $p53^{-/-}$, and E2F-$1^{-/-}$ mice. Indeed, transgenic expression of the RbAp48 gene induced apoptosis in the exocrine glands but not in other organs. These findings indicate that estrogen deficiency initiates p53-mediated apoptosis in the exocrine gland cells through RbAp48 overexpression and exerts a possible gender-based risk of autoimmune exocrinopathy in postmenopausal women.

Estrogenic action has been suggested to be responsible for the strong female preponderance of many autoimmune diseases, including systemic lupus erythematosus, rheumatoid arthritis, and Sjögren's syndrome (50, 51). Recent evidence suggests that apoptosis plays a key role in the physiology and pathogenesis of various autoimmune diseases (2, 7, 19, 35, 42). We have demonstrated that estrogenic action influences target epithelial cells through Fas-mediated apoptosis in a murine model for Sjögren's syndrome (13). Recently, we found that tissue-specific apoptosis in the exocrine glands spontaneously occurring in estrogen-deficient mice may contribute to the development of autoimmune exocrinopathy (14). We speculate that antiestrogenic actions might be a potent factor in the formation of pathogenic autoantigens. It has been reported that the antiestrogen tamoxifen (TAM) induces cell death in the human breast cancer cell line MCF-7 (17). We observed a time- and concentration-dependent increase in apoptosis of mouse and human salivary gland cells ([MSG] mouse primary culture; [HSG] human cell line) treated with TAM but not in other cell lines (HT-29, Colo201, and Jurkat) (14).

Apoptosis can be initiated by many different factors, but activation of caspases, which are a special class of proteolytic enzymes, is always involved in this process. Activation of caspases may be achieved by several molecular pathways; the best known stimuli triggering the caspase cascade are stimulation of Fas or TNF receptors, release of cytochrome *c* from the cellular mitochondria, and exposure to granzymes, which are secreted by cytotoxic T cells (3, 12, 31, 37, 54). Detailed research on the mechanisms controlling caspase activity will provide better insight into the pathogenesis of autoimmune diseases with special reference to estrogen deficiency. In this study, we have focused on the molecular mechanisms responsible for tissue-specific apoptosis caused by estrogen deficiency and identified RbAp48 as a novel apoptosis-inducing gene exclusively in the exocrine glands. Retinoblastoma (Rb) protein is a multifunctional protein that binds to transcription factors and kinases to regulate both cell growth and apoptosis (11). Although recent data suggest that loss of Rb can cause apoptosis through derepression of basally inhibited extrinsic apoptotic pathway genes (20), no mechanism has provided a molecular explanation for RbAp48 in the induction of apoptosis.

* Corresponding author. Mailing address: Department of Oral Molecular Pathology, Institute of Health Biosciences, The University of Tokushima Graduate School, 3 Kuramotocho, Tokushima 770-8504, Japan. Phone: 81 88 633 7327. Fax: 81 88 633 7327. E-mail: hayashi@dent.tokushima-u.ac.jp.

MATERIALS AND METHODS

Cell culture and gene transfection. HSG, MSG, HT29, Colo201, HeLa, HepG2, SH-SY5Y, NEC14, THP-1, Jurkat, Raji, U937, and W138 cells were cultured in Dulbecco's modified Eagle medium (DMEM) or RPMI 1640 medium containing 10% fetal bovine serum at 37°C. HSG and MSG cells have been described elsewhere (38, 40). The following were used for cell cultures: 10^{-7} M TAM (Wako Pure Chemical, Osaka, Japan), 10^{-9} M β-2-estradiaol (E2; Wako), 10^{-7} M staurosporin (Wako), paclitaxel (Wako), 1 μM etoposide (Wako), 1 μM ICI182780 (Wako), 25 ng/ml anti-Fas monoclonal antibody (MAb) (MBL, Nagoya, Japan), and 10 ng/ml recombinant human gamma interferon (R&D Systems, Minneapolis, MN). The RbAp48 gene inserted into the pCMV (2N3T) vector, a gift from D. Trouche, was transfected into the cells using FuGENE6 Transfection Reagent (Roche Diagnostics Corp., Indianapolis, IN). The RbAp48-stable cell line (RH0) from HSG cells in which RbAp48 expression was regulated by isopropyl-1-thio-β-D-galactopyranoside (IPTG), was established using a LacSwitch II Inducible Mammalian Expression System (Stratagene, La Jolla, CA). Briefly, the repressor vector (pCMVLacI) and RbAp48-inserted operator vector (pOPRVI/MCS) were cotransfected into HSG cells with FuGENE6, and the RbAp48 expression of hygromycin and G418-resistant transfectants was controlled by IPTG. For infection of adenovirus vector, RbAp48 gene-transfected MSG cells from $p53^{-/-}$ or wild-type mice were infected with 100 multiplicities of infection of adenovirus vector including the p53 gene obtained from Toren Finkel (National Institutes of Health). MSG and mouse mammary glands (MMG) were removed, placed in DMEM containing 10% fetal calf serum (FCS) and 10 mM HEPES (pH 7.4), and rapidly minced. The mate-

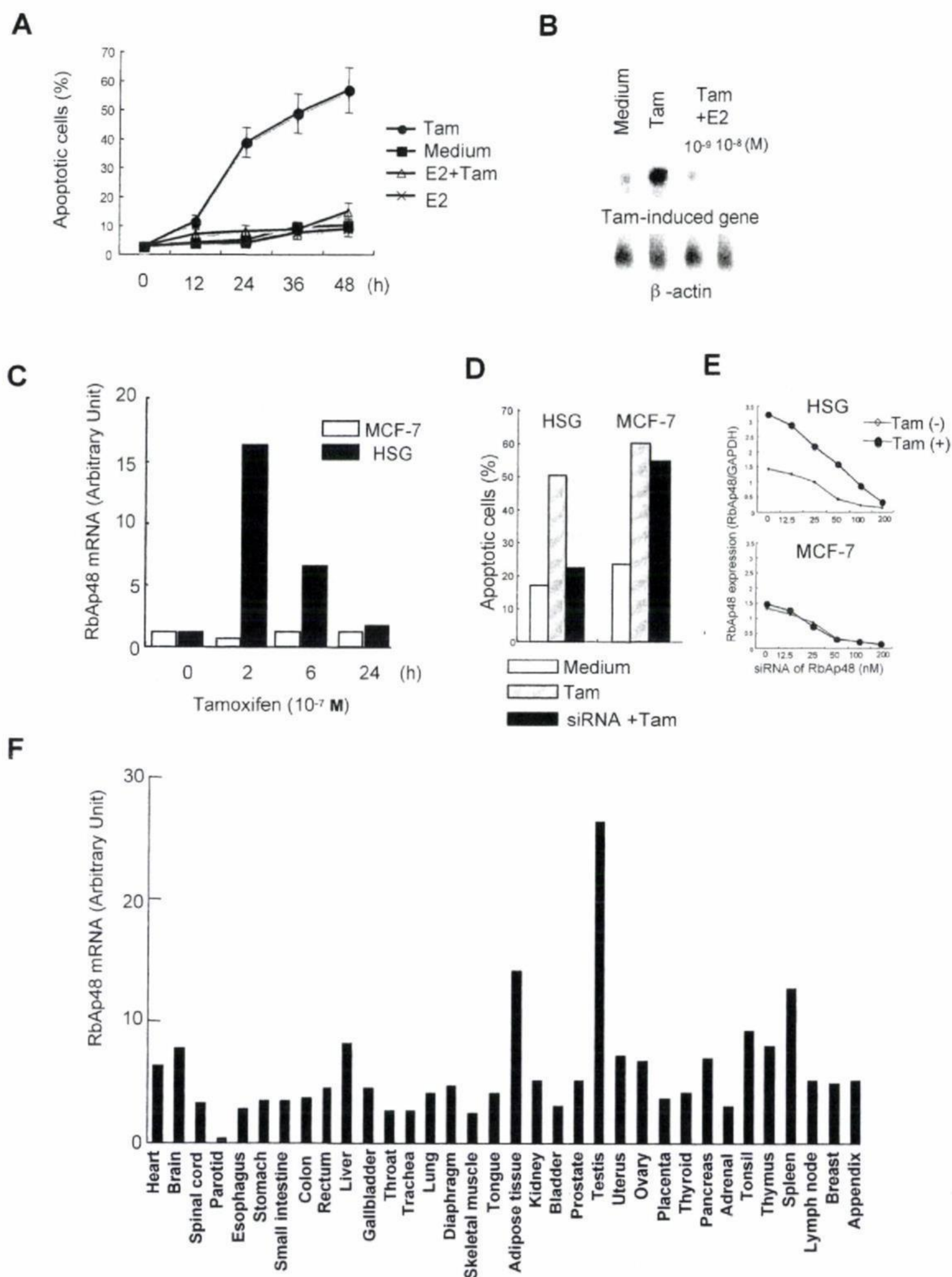

FIG. 1. Identification of the RbAp48 gene in salivary gland cell apoptosis. (A) A time-dependent increase in apoptotic HSG cells stimulated with TAM (10^{-7} M) was observed, and E2 (10^{-9} M) treatment inhibited apoptosis. Apoptotic cells were detected by flow cytometry using FITC-conjugated annexin V. (B) TAM-induced gene fragments cloned by differential display PCR were used as a probe by Northern blotting with mRNA from HSG cells treated with TAM (10^{-7} M) or E2 (10^{-9}M and 10^{-8}M). β-Actin mRNA was detected as an internal control. Each blot is representative of three independent experiments. (C) Analysis of RbAp48 mRNA expression was performed using total RNA from TAM-stimulated HSG and MCF-7 cells for 0 to 24 h. The graph is representative of three independent experiments. (D) The inhibitory effects of siRNA on TAM-induced apoptosis in HSG cells with siRNA (15 nM) of the RbAp48 construct but not in MCF-7 cells. After transfection of siRNA of RbAp48 and a fluorescence-labeled control gene, the cells were incubated with TAM (10^{-7} M) for an additional 24 h. Apoptosis was estimated by flow cytometric analysis using PE-conjugated annexin V. The graph is representative of three independent experiments. (E) A dose-dependent inhibition of siRNA (0 to 200 nM) of TAM-induced RbAp48 expression in HSG cells, not MCF-7 cells, was observed. The graph is representative of two independent experiments. (F) RbAp48 mRNA expression levels were analyzed using human tissue total RNA-blotted membrane. Message levels (arbitrary units) were quantified by BAS-2000II and expressed as the ratio of RbAp48 mRNA/β-actin mRNA. The graph is representative of two independent experiments.

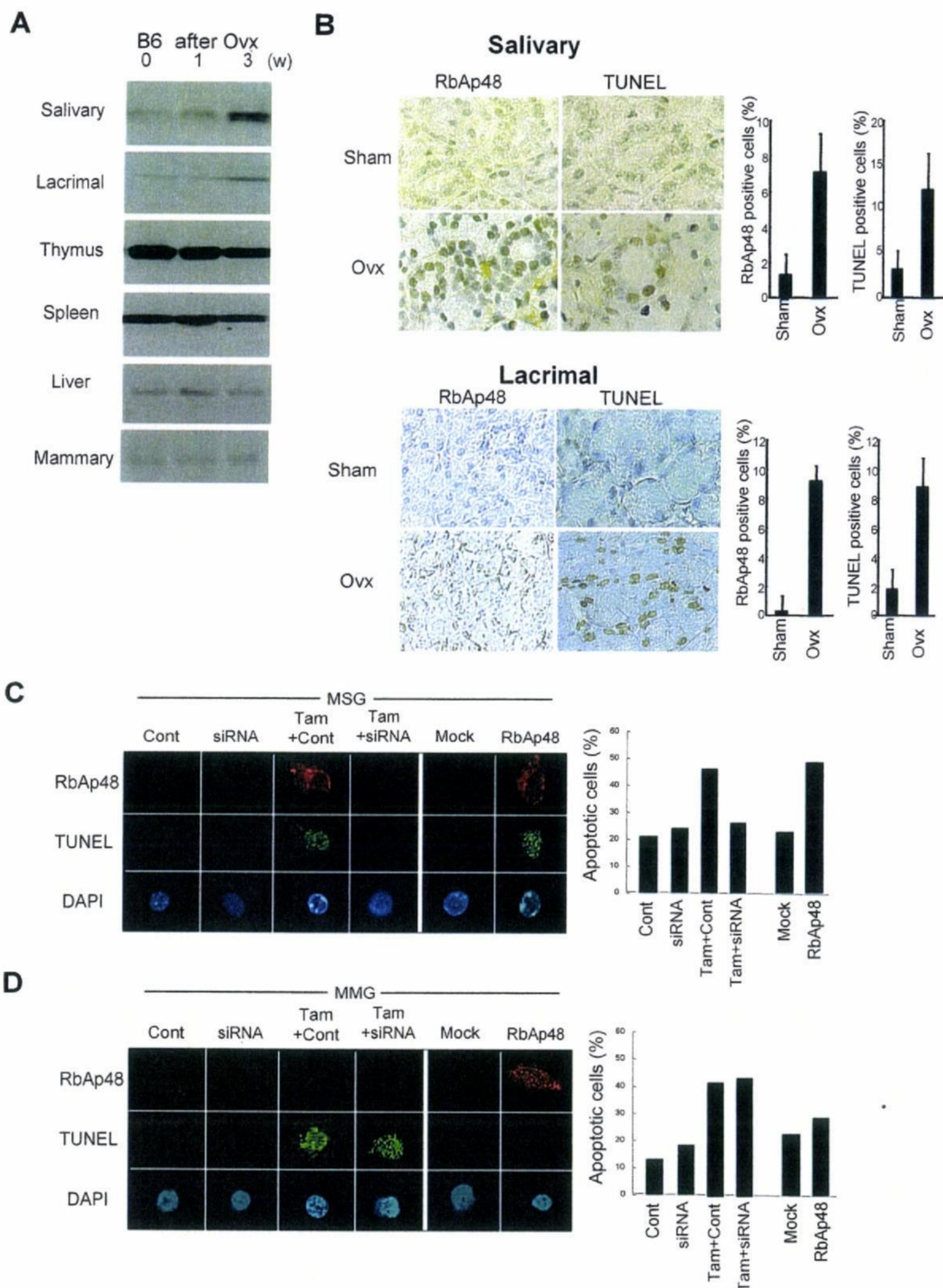

FIG. 2. RbAp48 overexpression in OVX B6 mice. (A) Increased RbAp48 expression in salivary and lacrimal gland tissues in OVX B6 mice from 0 to 3 weeks (age of mice, 4 to 7 weeks). Expression levels of RbAp48 in thymus, spleen, liver, and mammary glands from OVX B6 mice were constant. Western blot analysis was performed on proteins from tissue homogenates of OVX and sham mice. Blots were representative of three independent experiments. (B) Detection of RbAp48$^+$ and TUNEL$^+$ cells in salivary and lacrimal glands from OVX B6 and sham B6 mice at the age of 7 weeks. Immunohistochemical analysis of RbAp48 and in situ TUNEL assays were performed on the sections of salivary and lacrimal glands from OVX and sham mice. Images are representative of sections from five mice. The percentage of RbAp48$^+$ and TUNEL$^+$ cells in salivary and lacrimal glands was enumerated using a 10- by 20-mm grid covering an objective area of 0.16 mm^2. Data were analyzed in 10 fields per section and expressed as mean percent ± standard deviation of data from five mice. (C) TAM-induced apoptosis was associated with RbAp48 expression in

rials were then digested for 1 h at 37°C with 750 U/ml collagenase (Wako), 500 U/ml hyarulonidase type IV (Sigma), 1% bovine serum albumin, and 10 mM HEPES (pH 7.4) in DMEM. After digestion, they were filtered through a 70-μm nylon mesh, centrifuged, and rinsed twice with DMEM containing 10% FCS. These cells were cultured in chamber slides (Nalge Nunc International, Denmark) at a density of 5×10^4/well with DMEM containing 10% FCS. After cells were cultured for 24 h, the medium was changed to HuMedia-KG2 (Kurabo, Osaka, Japan).

Differential display analysis and Northern blotting. Total RNA was isolated from TAM-treated or nontreated HSG cells and reverse transcribed for differential display PCR with an RNAimage kit (Gene Hunter, Nashville, TN). TAM-induced cDNA fragments were gel excised and subcloned for TA vector. The clones were screened with a cDNA library derived from mRNA of TAM-stimulated HSG cells. The screened clone was transformed to plasmid and sequenced. Expressions of RbAp48 mRNA were detected by Northern blot analysis using ^{32}P-labeled RbAp48 cDNA probe. Equal loading of the gel was confirmed by using β-actin cDNA probe. In addition, the human total RNA-blotted membrane (Biocain Institute, Inc., San Leandro, CA) was used for analysis of RbAp48 mRNA in various human tissues.

Apoptosis detection assay. Apoptosis was detected using the annexin V-fluorescein isothiocyanate (FITC) apoptosis detection kit (Genzyme Corp., Cambridge, MA). Briefly, after cultured cells were washed with phosphate-buffered saline, the cells were incubated with FITC-conjugated annexin V and propidium iodide (PI) for 10 min at room temperature in the dark. Binding buffer was added, and apoptotic cells were detected by flow cytometric analysis with an EPICS flow cytometer (Beckman Coulter, Inc., Miami, FL).

Mice. Estrogen receptor α-deficient (ERα$^{-/-}$), p53$^{-/-}$, E2F-1$^{-/-}$, or C57BL/6 (B6) mice were purchased from Taconic (Germantown, NY), Jackson Laboratory (Bar Harbor, ME), or Nihon Clea (Tokyo, Japan). These mice were subjected to ovariectomy (OVX mice) and or to a sham operation (sham mice) at 4 weeks of age. At 0 to 3 weeks after OVX, all organs were evaluated by pathological or immunohistochemical analysis. To generate the RbAp48-transgenic (TG) mice, B6 mice were used to obtain fertilized eggs, and the gene fragment containing RbAp48 cDNA regulated by salivary gland-specific promoter (22) (provided by B. B. Larsen) was microinjected into the pronucleus of fertilized eggs to establish the transgenic lines. Histopathological analysis of all organs of RbAp48-TG mice screened by PCR was performed. All mice were maintained in our specific-pathogen-free facility.

siRNA of RbAp48. Small interfering RNA (siRNA) corresponding to the coding sequence +136 to +156 of the RbAp48 gene was synthesized by Hokkaido System Science (Sapporo, Japan) according to standard methods (23, 52) for the following: sense, CGAGGAAUACAAAAUAUGGTT; antisense, CCA UAUUUUGUAUUCCUCGTT. siRNA of the glyceraldehyde-3-phosphate dehydrogenase (GAPDH) gene (Ambion, Austin, TX) was used as a control. siRNA (0 to 50 nM) and 1 μg of pCMV-green fluorescent protein (GFP) plasmid were cotransfected into HSG, MCF-7 cells, and the IPTG-controlled RbAp48-stable cell line (RH0) using a Silencer siRNA Transfection II Kit (Ambion) or FuGENE6 (Roche). At 24 h after cotransfection, RH0 cells were incubated with IPTG for an additional 24 h. GFP$^+$ apoptotic cells were detected by flow cytometry using phycoerythrin (PE)-conjugated annexin V.

E2F-1, ARF, and p53 siRNA. For siRNA of E2F-1, ARF, and p53, an siTrio Full Set (B-Brigde International, Sunnyvale, CA) was used for HSG cells. Briefly, each cocktail including the three RNA oligonucleotides listed below was transfected into cells with a Quick-Step Transfection Kit (B-Brigde International). Sequences of the oligonucleotide sets are as follows: for E2F-1, CCAACGUCCU UGAGGGCAUTT (sense), AUGCCCUCAAGGACGUUGGTT (antisense), CU GCAGAGCAGAUGGUUAUTT (sense), AUAACCAUCUGCUCUGCAGTT (antisense), GGAAAGUGAGGGAGGGAGATT (sense), and UCUCCCUCCC UCACUUUCCTT (antisense); for ARF, GCUCACCUCUGGUGCCAAATT (sense), UCACCAAGAACCUGCGCACTT (antisense), GGGUUUUCGCGGU UCACAUTT (sense), AUGUGAACCACGAAAACCCTT (antisense), GGGUU UUCGUGGUUCACAUTT (sense), and AUGUGAACCACCACGAAAAC CCTT (antisense), for p53, GGAAACUACUUCCUGAAAATT (sense), UUUU CAGGAAGUAGUUUCCTT (antisense), CUGGAAGACUCCAGUGGUATT (sense), UACCACUGGAGUCUUCCAGTT (antisense), CUUAGUACCUAAA AGGAAATT (sense), and UUUCCUUUUAGGUACUAAGTT (antisense). Transfected cells were incubated with or without TAM, and confocal or flow cytometric analysis was performed.

Western blotting. Whole-cell extracts of HSG or RH0 cells were purified using radioimmunoprecipitation assay buffer (50 mM Tris-HCl, pH 7.4, 150 mM NaCl, 1 mM EDTA, 1% NP-40, 1 mM dithiothreitol [DTT], 1 mM phenylmethylsulfonyl fluoride) supplemented with a protease inhibitor cocktail (Sigma Chemical Co., St. Louis, MO). After centrifugation for 20 min at 12,000 rpm at 4°C, the supernatant was extracted and used for samples. Also, to detect α-fodrin in organs, tissue samples from OVX and sham C57BL/6 mice were extracted as described above. Ten micrograms of each sample per well was used for 7.5 to 12.5% sodium dodecyl sulfate-polyacrylamide gel electrophoresis and transferred to polyvinylidene difluoride membranes, which were probed with anti-RbAp48, anti-Rb (p110 and p130), anti-Bad, anti-Bax, anti-ARF (p14 and p19), anti-cyclin D3 (BD Transduction Laboratories, Lexington, KY), anti-Mdm2, anti-E2F-1, anti-phospho-Rb (Sigma), anti-p53, anti-phospho-p53 Ab sampler kit (Ser6, Ser9, Ser15, Ser20, Ser37, Ser46, and Ser392; Cell Signaling Technology Inc., Beverly, MA), anti-α-fodrin (Affiniti, Mamhead, United Kingdom), and anti-p21 (Santa Cruz Biotechnology, Santa Cruz, CA) as the primary Abs, and anti-α-tubulin, GAPDH, or histone MAb (Sigma) as internal control. The nitrocellulose membranes were incubated with peroxidase-conjugated horse anti-mouse or rabbit immunoglobulin G (IgG; Vector Laboratories) as the secondary Ab. Protein binding was visualized with ECL Western blotting reagent (Amersham Corp., Arlington Heights, IL).

TUNEL assay. Apoptotic cells were detected in sections using the in situ terminal deoxynucleotidyltransferase (TdT)-mediated dUTP-biotin nick end labeling (TUNEL) kit (Wako). Sections were incubated with proteinase K (20 μg/ml) for 10 min and then presoaked in TdT buffer (0.5 μM cacodylate, 1 mM CoCl, 0.5 μM DTT, 0.05% bovine serum albumin, 0.15 M NaCl) for 10 min. Sections were incubated for 2 h at 37°C in 25 μl of TdT solution, containing 1× terminal transferase buffer, 0.5 nmol of biotin-dUTP, and 10 U of TdT. After the TdT reaction, sections were soaked in TdT blocking buffer (300 nM NaCl, 30 mM Tris-sodium citrate-2-hydrate), incubated with horseradish peroxidase-conjugated streptavidin for 30 min at room temperature, and developed for 10 min in phosphate-buffered citrate (pH 5.8) containing 0.6 mg/ml DAB (3,3′-diaminobenzidine-tetrahydrochloride-dihydrate). Nuclei were counterstained with hematoxylin. For confocal microscopic analysis, FITC-labeled UTP was used.

Caspase activity assay. Caspase activities were assayed using a caspase family colorimetric substrate set (BioVision Inc.). Briefly, 100 μg of cytoplasmic lysates of RH0 cells was incubated with 200 μM Ac-YVAD-pNA (caspase 1 substrate), Ac-VDVAD-pNA (caspase 2 substrate), Ac-DEVD-pNA (caspase 3 substrate), Ac-WEHD-pNA (caspase 5 substrate), Ac-VEID-pNA (caspase 6 substrate), Ac-IETD-pNA (caspase 8 substrate), and Ac-LEHD-pNA (caspase 9 substrate) at 37°C for 1 h. The absorbance of samples was read at 405 nm in a microtiter plate reader. The relative percent increase in caspase activity was determined by comparing these results with the level of the uninduced control.

Gel shift assay. Nuclear extracts were prepared from RH0 cells by a method previously described (29). Nuclear extracts containing 5 μg of protein were incubated in 20 μl of binding buffer (10 mM Tris-HCl, pH 8.0, 50 mM NaCl, 1 mM MgCl2, 0.5 mM DTT, and 4% glycerol) with or without a cold competitor. The E2F-1 DNA probe, 5′-TCCGTAGTTTTCGCGCTTAAATTTGAGAAAG GGCGCGAAACTAGTC-3′ (10,000 cpm) labeled with [γ-^{32}P]ATP was added, and the samples were incubated at room temperature for 20 min. Reaction mixtures were separated in a 4% polyacrylamide gel and autoradiographed on X-ray film (Fujifilm, Kanagawa, Japan).

Immunohistochemical analysis. Immunohistochemical analysis of RbAp48 expression was performed on the sections of salivary and lacrimal glands from sham, OVX B6, RbAp48-WT (wild type), and RbAp48-TG mice. Paraffin-embedded sections were stained with anti-RbAp48 MAb (BD Transduction Laboratories) as the primary Ab. Protein binding was detected with an LSAB2 kit containing horseradish peroxidase (DAKO, Carpineteria, CA) and DAB as a substrate. The counterstaining of nuclei was performed with hematoxylin.

Confocal microscopy. Confocal microscopic analysis of RbAp48, E2F-1, ARF, and p53 expression, and TUNEL-positive cells was performed on the cultured cells, and frozen sections of salivary glands from sham, OVX ERα$^{-/-}$, p53$^{-/-}$,

MSG cells from B6 mice, and the inhibitory effects with siRNA of RbAp48 construct were observed by confocal microscopic analysis. The percentage of TUNEL$^+$ apoptotic cells was enumerated as described. Cont, irrelevant siRNA control. Images are representative of three independent experiments. (D) TAM-induced apoptosis was not associated with RbAp48 expression in the primary culture of MMG cells from B6 mice. TUNEL$^+$ apoptotic cells were enumerated as described. Images are representative of three independent experiments.

$E2F1^{-/-}$, RbAp48-WT, and RbAp48-TG mice using a Confocal Laser Microscan (LSM 5 PASCAL; Carl Zeiss, Germany). As the second Abs, Alexa Fluor 488–anti-mouse IgG heavy and light chain [IgG (H+L)], Alexa Fluor 568–goat anti-rabbit IgG (H+L), Alexa Fluor 488–donkey anti-rat IgG (H+L), Alexa Fluor 488–chicken anti-goat IgG (H+L), and Alexa Fluor 568–rabbit anti-goat IgG (H+L) were used. Nuclear DNA was stained with 4',6-diamidino-2-phenylindole dihydrochloride.

BrdU incorporation. MSG cells from RBAp48 TG and WT mice were stimulated with phorbol 12-myristate 13-acetate for 24 h, and 10 mM bromodeoxyuridine (BrdU) was incorporated for the last 2 h. Fixed and permeabilized cells were treated with DNase and stained with FITC-conjugated anti-BrdU antibody (BD Pharmingen, San Diego, CA). The polyvinylidene difluoride DNA synthetic activity was analyzed by flow cytometry.

RESULTS

Identification of TAM-induced gene. We found a time-dependent increase in apoptotic HSG cells stimulated with TAM, and E2 treatment inhibited the apoptosis (Fig. 1A). To identify gene products specific to TAM-induced apoptosis in the salivary gland cells, mRNAs from HSG cells treated with TAM and nontreated cells were analyzed by a differential display PCR method. From the samples isolated with the highest grade of differential expression, we analyzed the mRNAs from HSG cells treated with TAM and nontreated cells by a reverse Northern blotting technique (Fig. 1B). The sequence of TAM-induced mRNA corresponds (100%) to RbAp48. The expression of RbAp48 mRNA in HSG cells reached peak level at 2 h after stimulation with TAM, and then the level decreased, whereas increased expression of RbAp48 mRNA in MCF-7 cells was not observed (Fig. 1C). We confirmed the inhibitory effects of siRNA on TAM-induced apoptosis in HSG cells, not MCF-7 cells, with siRNA (5 to 50 nM) of RbAp48 construct (Fig. 1D). In addition, a dose-dependent inhibition of siRNA (0 to 200 nM) on TAM-induced RbAp48 expression in HSG cells, not MCF-7 cells, was observed (Fig. 1E). We next searched the tissue distribution of RbAp48 mRNA using human tissue total RNA-blotted membrane by Northern blot analysis. We found the highest level of expression of RbAp48 mRNA in the testis, which is consistent with the previous report (33), and the lowest was found in the parotid salivary gland (Fig. 1F), although the molecular mechanism by which the lowest RbAp48 mRNA is expressed in the parotid glands is unclear.

RbAp48 overexpression in estrogen-deficient mice. To confirm the in vivo overexpression of RbAp48 and apoptosis in estrogen-deficient B6 mice, OVX was performed on mice at the age of 4 weeks. Using Western blotting, we detected a time-dependent increase in RbAp48 in the salivary and lacrimal gland tissues from 0 to 3 weeks after OVX (at the age of 4 to 7 weeks) but not in other organs, including mammary glands (Fig. 2A). $RbAp48^{+}$ and $TUNEL^{+}$ apoptotic cells were detected by immunohistochemical analysis in the salivary and lacrimal gland sections from OVX B6 mice at the age of 7 weeks but not in sham mice (Fig. 2B). In vitro studies using primary cultured cells from B6 mice demonstrated that TAM-induced apoptosis was associated with RbAp48 expression in MSG cells but not in MMG cells (Fig. 2C and D). We confirmed the inhibitory effects of siRNA in MSG cells but not in MMG cells with siRNA of RbAp48 construct (Fig. 2C and D).

RbAp48 as a novel apoptosis-inducible gene. RbAp48 mRNA expression and apoptosis could be induced in HSG cells stimulated with TAM and a pure antiestrogen, ICI182780, but not with other apoptotic stimuli such as staurosporin, paclitaxel, anti-Fas MAb, and etoposide (Fig. 3A). This indicates that induction of RbAp48 mRNA expression might be dependent on estrogen deficiency. To ensure the role of RbAp48 in various types of cells, RbAp48 was transiently transfected, and apoptosis was determined by flow cytometry using an annexin V-FITC apoptosis detection kit. Among the cells examined (HSG, MSG, MCF-7, HT-29, Colo201, HeLa, HepG2, SH-SY5Y, NEC14, THP-1, Jurkat, Raji, U937, and WI38), significant apoptosis was induced exclusively in the salivary gland cells transfected with RbAp48 of both human and mouse origin (Fig. 3B). Notably, apoptosis was induced by transfection with RbAp48 cDNA in MSG cells isolated from $ER\alpha^{-/-}$ mice, indicating that this signaling might act in the downstream of estrogen-ER binding. Apoptotic cells could not be induced by the transgene of RbAp48 cDNA but was induced by TAM in MCF-7 cells. We confirmed that the induction levels of RbAp48 are the same in the other cell lines including Jurkat and THP-1 as the HSG cells (Fig. 3C). We next generated and analyzed the RbAp48-stable cell line (RH0), which was an IPTG-inducible transfectant of RbAp48 in HSG cells, with a LacSwitch II Inducible Mammalian Expression System using repressor and operator vectors. Apoptosis was drastically induced in IPTG-treated RH0 cells in association with RbAp48 expression within 8 h (Fig. 3D). When we examined the effect of siRNA on RbAp48-induced apoptosis, the apoptosis in IPTG-treated RH0 cells was clearly inhibited by siRNA of RbAp48 but not by siRNA of GAPDH or an irrelevant control (Fig. 3E).

Molecular mechanisms for RbAp48-induced apoptosis. We next examined the molecular mechanisms responsible for RbAp48-induced apoptosis. We detected upregulation of phosphorylated Rb, cyclin D3, p14ARF, Bax, Bad, cytochrome *c* (Cyt *c*) and a cleavage product of α-fodrin (arrow) in IPTG-treated RH0 cells (Fig. 4A). Our previous report demonstrated that α-fodrin is a candidate autoantigen of primary Sjögren's syndrome (10). When nuclear extracts of IPTG-treated RH0 cells were analyzed by gel shift assay, DNA binding activity of E2F-1 was detected in RbAp48-induced apoptotic cells (Fig. 4B). E2F-1 protein was also detected in the nuclear extract by Western blotting (Fig. 4B). It has been proposed that the E2F-1 transcription factor serves as a link between the Rb/E2F proliferation pathway and the p53 apoptosis pathway by inducing the expression of p14ARF, a protein that regulates p53 stability (36). We next focused on the p53-dependent pathway, because MSG cells transfected with RbAp48 isolated from $p53^{-/-}$ mice are apoptosis resistant (Fig. 4C). When Adp53-infected MSG cells were transfected with the RbAp48 gene, apoptosis was rapidly induced (Fig. 4C). Phosphorylated p53 (Ser9) was found by Western blotting after 2 to 4 h, but no other phosphorylated p53 (Ser15, Ser20, and Ser392) was detected (Fig. 4D). The phosphorylation of p53 in the other sites (Ser6, Ser37, and Ser46) was not observed (data not shown). We also confirmed a time-dependent downregulation of Mdm2 (Fig. 4D), which is important as a regulatory partner of p53 (47). Using Western blotting, we also detected increased p21 expression, a major player in the p53-mediated pathway, in IPTG-treated RH0 cells (Fig. 4E). p53 induces apoptosis by a multitude of molecular pathways, in addition to transactivation

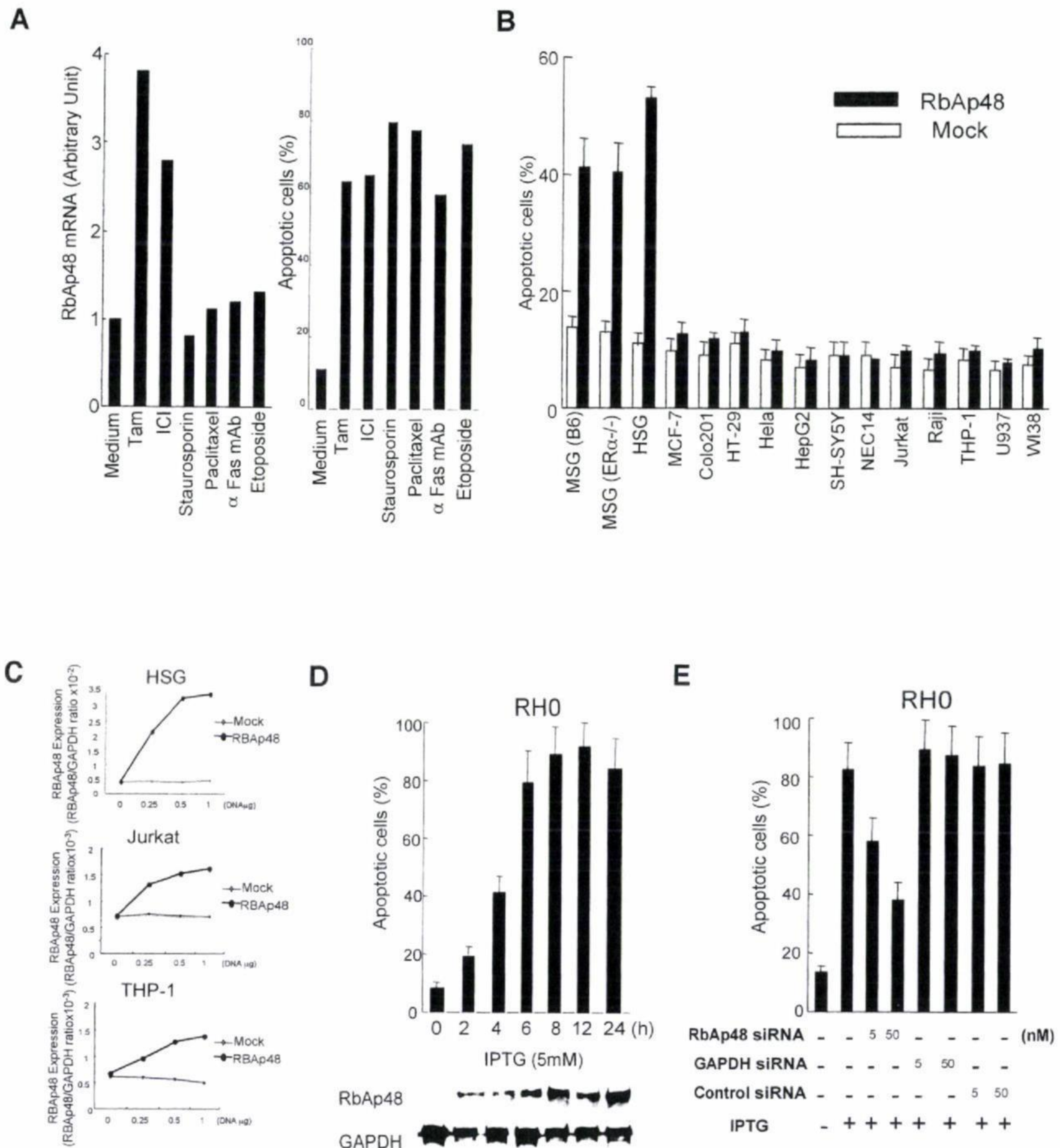

FIG. 3. Role of RbAp48 in salivary gland cell apoptosis. (A) HSG cells were treated with antiestrogenic reagents (10^{-7} M TAM and 10^{-7} M ICI182780) and general apoptotic stimuli (staurosporin, paclitaxel, anti-Fas MAb, and etoposide). RbAp48 mRNA was quantitated with BAS-2000II, and message level was expressed as the ratio of RbAp48 mRNA/β-actin mRNA; the percentage of apoptotic cells was detected by FITC-annexin V-PI was expressed for all of these agents. Graphs are representative of three independent experiments. (B) The RbAp48 gene was transiently transfected into various cells using FuGENE6. At 48 h after transfection of pCMV-RbAp48 plasmid or pCMV (mock) plasmid, apoptotic cells were detected by FITC-annexin V-PI. Data are the means ± standard deviations of triplicate samples. The graph is representative of three independent experiments. (C) The levels of the induction ratio of RbAp48 were shown to be the same in the other cell lines including Jurkat and THP-1 as the HSG cells using Western blot analysis. The levels were expressed as the ratio of RbAp48/GAPDH protein. (D) Establishment of the RbAp48 stable cell clone. An increase in RbAp48 expression and apoptosis of IPTG-treated RH0 cells were observed in a time-dependent manner. Apoptotic cells were detected by FITC-annexin V-PI. Data are means ± standard deviations of triplicate samples. Expressions of RbAp48 and GAPDH as an internal control were detected by Western blot analysis. Graph and images are representative of four independent experiments. (E) Inhibitory effects of siRNA on RbAp48-induced apoptosis. IPTG-treated RH0 cells were cotransfected with siRNA (5 to 50 nM) of RbAp48 and pCMV-GFP. Apoptotic cells gated on GFP^{+} were detected by PE-conjugated annexin V. Data are means ± standard deviations of triplicate samples. Graph is representative of three independent experiments.

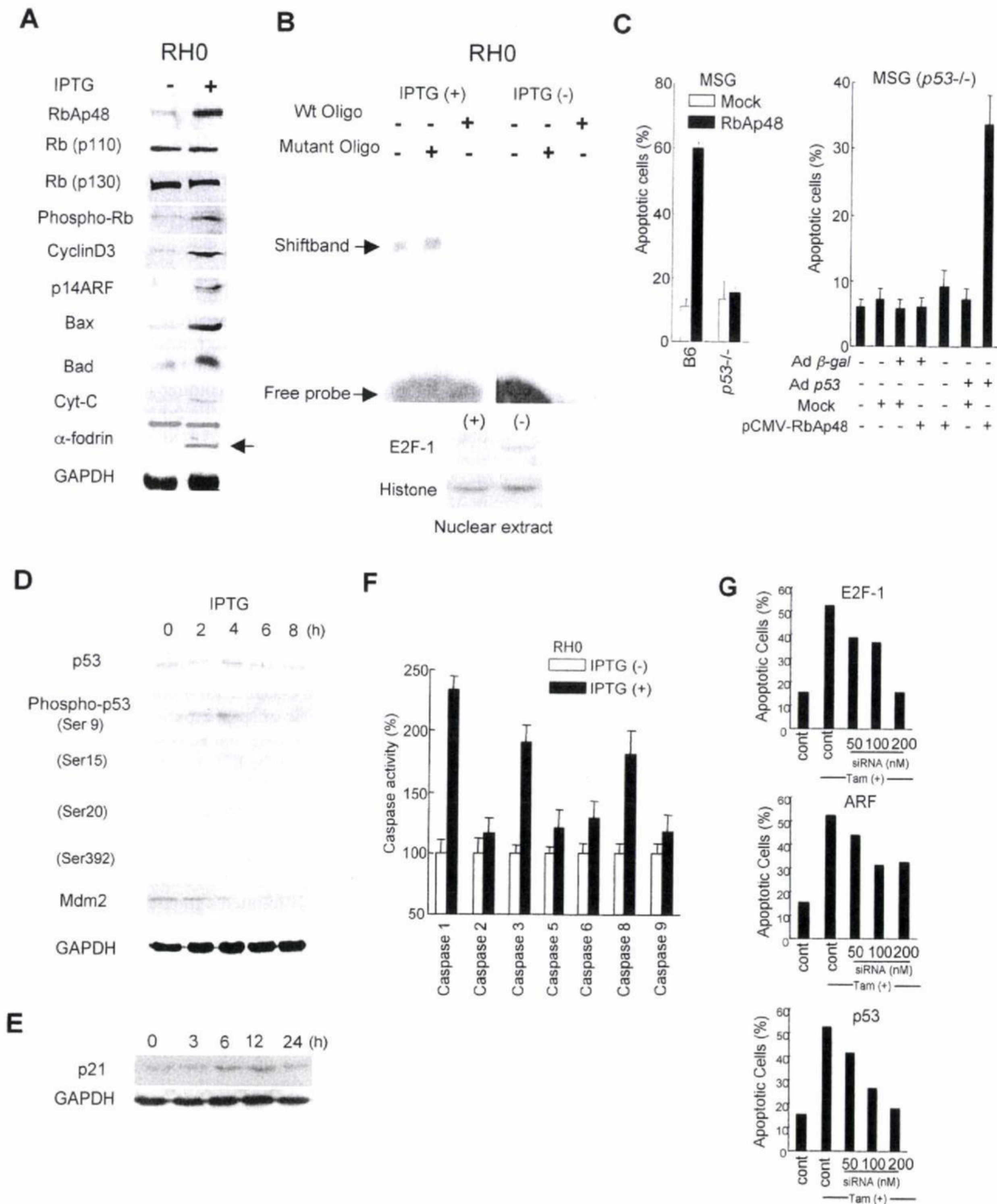

FIG. 4. Molecular mechanisms responsible for RbAp48-induced apoptosis. (A) Contribution of cell cycle and mitochondrion-related molecules in RbAp48-induced apoptosis of RH0 cells. The lysates of IPTG-treated or nontreated RH0 cells were used to detect RbAp48, Rb (p110 and p130), phospho-Rb, cyclin D3, p14ARF, Bax, Bad, Cyt-*c*, the cleavage product of α-fodrin, and GAPDH for Western blot analysis. Blots are representative of three independent experiments. (B) Detection of E2F-1 transcriptional activity in RbAp48-induced apoptosis. The nuclear proteins of IPTG-treated RH0 cells were analyzed by gel shift assay with an E2F-1 binding DNA probe. To confirm the specific binding to the E2F-1 binding site, the mutant oligonucleotide and wild-type oligonucleotide as a competitor were used for this assay. E2F-1 protein was detected in the nuclear extract by Western blotting. Histone was used for an internal control. Blots are representative of three independent experiments. (C) Apoptosis of MSG cells from $p53^{-/-}$ mice was not observed by RbAp48 gene transfection. Transfection with pCMV (Mock) was used as control. MSG ($p53^{-/-}$) cells were infected with Ad*p53* and incubated for 24 h. The infected cells were cotransfected with the RbAp48 gene and

of target genes, and it can elicit apoptosis by transcription-independent mechanisms (5, 28). Although apoptosis in response to p53 activation is often accompanied by caspase activation, the mechanisms underlying p53-induced caspase activation remain poorly understood. Caspase activities in RbAp48-induced apoptosis in HSG cells were assayed using a caspase family colorimetric substrate set. A significant increase in caspase 1 activity was detected with relatively elevated caspase 3 and 8 activity on RbAp48-induced apoptotic HSG cells (Fig. 4F). RbAp48-induced apoptosis in HSG cells was clearly inhibited by siRNA of E2F-1 and p53 but only moderately by siRNA of ARF (Fig. 4G).

RbAp48/E2F1/ARF-p53 pathway in the salivary glands. We evaluated the effects of RbAp48 overexpression and knockdown in primary MSG cells and documented the effects on E2F-1, ARF, and p53 protein levels in these cells. We demonstrated that overexpression of RbAp48 in MSG cells from B6 mice induced E2F-1, p19ARF, and phospho-p53 expression, and the inhibitory effect of siRNA of RbAp48 was observed from confocal microscopic analysis (Fig. 5A). We next examined whether TAM-induced apoptosis is associated with RbAp48 expression in MSG cells from B6 mice, compared with cells from $ER^{-/-}$, $E2F1^{-/-}$, and $p53^{-/-}$ mice. By confocal microscopic analysis, we found that TAM-induced apoptosis was associated with RbAp48 expression in MSG cells from B6 mice but not from $ER^{-/-}$, $E2F1^{-/-}$, and $p53^{-/-}$ mice Fig. (5B). We further examined the effect of OVX on the expression of RbAp48, E2F-1, p19ARF, and phospho-p53 in MSG cells from B6, $ER^{-/-}$, $E2F1^{-/-}$, and $p53^{-/-}$ mice. By double-labeled confocal microscopy, we found coexpression of RbAp48/E2F1, RbAp48/p19ARF, and RbAp48/p53 in MSG cells from OVX B6 mice but not from B6 mice (Fig. 5C). No differences in RbAp48/E2F1, RbAp48/p19ARF, and RbAp48/phospho-p53 expression levels were observed in MSG cells from non-OVX and OVX $ER^{-/-}$, $E2F1^{-/-}$, and $p53^{-/-}$ mice (Fig. 5C).

Findings in RbAp48-transgenic mice. We constructed several lines of B6 background TG mice (39) expressing RbAp48 in the salivary glands using Lama promoter as described in Materials and Methods. Prominent expression of RbAp48 in the salivary glands from TG mice was determined at the age of 8 to 20 weeks by both immunohistochemistry and Western blotting (Fig. 6A and B). No difference in RbAp48 expression in the spleen was observed between TG and WT mice. A considerable number of $TUNEL^{+}$ apoptotic epithelial duct cells were found in the salivary glands of RbAp48-TG mice but not WT mice at the age of 20 weeks (Fig. 6C). In addition, expression of E2F-1, p19ARF, and phospho-p53 was observed in the salivary glands of RbAp48-TG mice but not WT mice (Fig. 6D). BrdU studies of TG mice with ectopic RbAp48 in the salivary glands demonstrated that cellular proliferation is barely affected (Fig. 6E). No pathological findings were observed in other organs of TG mice.

DISCUSSION

In this study, we demonstrated the first evidence that gender-based, tissue-specific apoptosis could be induced in the exocrine gland cells through RbAp48 overexpression with p53 phosphorylation. Indeed, RbAp48 overexpression with apoptosis was observed in the exocrine glands in OVX C57BL/6 mice, and transgenic expression of the RbAp48 gene induced tissue-specific apoptosis in the exocrine glands.

RbAp48, initially identified as a retinoblastoma binding protein (34), was characterized as a component of distinct nucleosome-modifying complexes, including the nuclear histone deacetylases (18, 25). In general, the functions of the RbAp48-like proteins in these complexes remain undetermined. It was reported that E2F-1 and RbAp48 are physically associated in the presence of Rb and histone deacetylase (26), suggesting that RbAp48 could be involved in transcriptional repression of E2F-responsive genes. The induction of apoptosis in various cell lines is accompanied by a shift in Rb from the hyper- to the hypophosphorylated form (49). Rb dephosphorylation, which has been shown to be required for apoptosis, occurs in the early stage of apoptosis (6). Loss of Rb function can induce p53-dependent apoptosis, but little is known about the mechanisms of Rb-regulated p53-dependent apoptosis. Recently, Lieman et al. provided evidence for a novel mechanism linking Rb-E2F to the extrinsic apoptotic pathway through inactivation of focal adhesion kinase and activation of caspase 8 (20). It has been proposed that the E2F-1 transcription factor serves as a link between the Rb/E2F proliferation pathway and the p53 apoptosis pathway by inducing the expression of p14ARF, a protein that regulates p53 stability. Recent observations have revealed that p53 can directly translocate to mitochondria and induce apoptosis in a transactivation-independent manner (21). In this study, we confirmed a time-dependent downregulation of Mdm2, which is important as a regulatory partner of p53 (47). In addition to regulation of p53, Mdm2 has been reported to stimulate E2F-1 transactivation by a mechanism that remains unclear. E2F-1 can signal p53 phosphorylation in the absence of p14ARF, similar to the observed modifications to p53 in response to DNA damage. p53 modification is found to be crucial for E2F-1-mediated apoptosis, and this apoptosis is compromised when E2F-1 is coexpressed with a p53 mutant

pCMV-GFP, and then apoptosis was detected by PE-annexin V on GFP^{+} cells. Infection of adenovirus β-galactosidase was used as a control. Graphs are representative of five independent experiments. (D) Expression levels of p53, phospho-p53 (Ser9), and Mdm2 in IPTG-treated RH0 cells. Other phosphorylated p53 proteins (Ser15, Ser20, and Ser392) were not detected. GAPDH expression was used for an internal control. Blots are representative of three independent experiments. (E) Detection of increased p21 expression, a major player in the p53-mediated pathway, by Western blotting. Blot is representative of two independent experiments. (F) Caspase activities of IPTG-treated RH0 cells were analyzed by a caspase enzymatic activity assay. A significant increase in caspase-1 activity was detected with relatively elevated caspase 3 and 8 activity. The absorbance of samples was read at 405 nm in a microtiter plate reader and the relative percent increase in activity was calculated by comparing the absorbance of IPTG-treated cells with that of untreated cells. Data are means ± standard deviations of triplicate samples. The graph is representative of three independent experiments. (G) RbAp48-induced apoptosis in HSG cells was clearly inhibited by siRNAs of E2F-1 and p53 but only moderately by siRNA of ARF. Graphs are representative of three independent experiments.

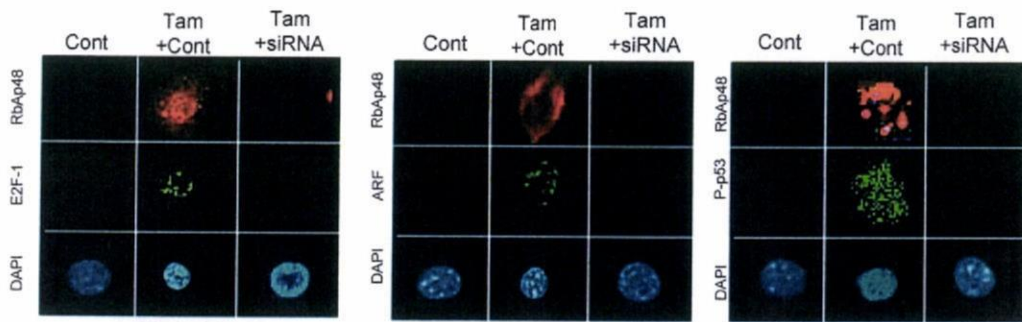
A
Cont
Tam +Cont
Tam +siRNA
RbAp48
E2F-1
DAPI
ARF
P-p53

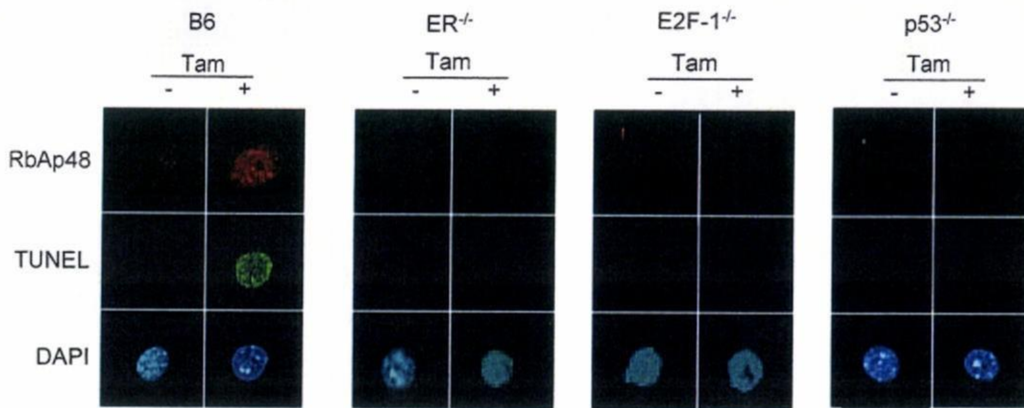
B
B6
$ER^{-/-}$
$E2F-1^{-/-}$
$p53^{-/-}$
Tam
-
+
RbAp48
TUNEL
DAPI

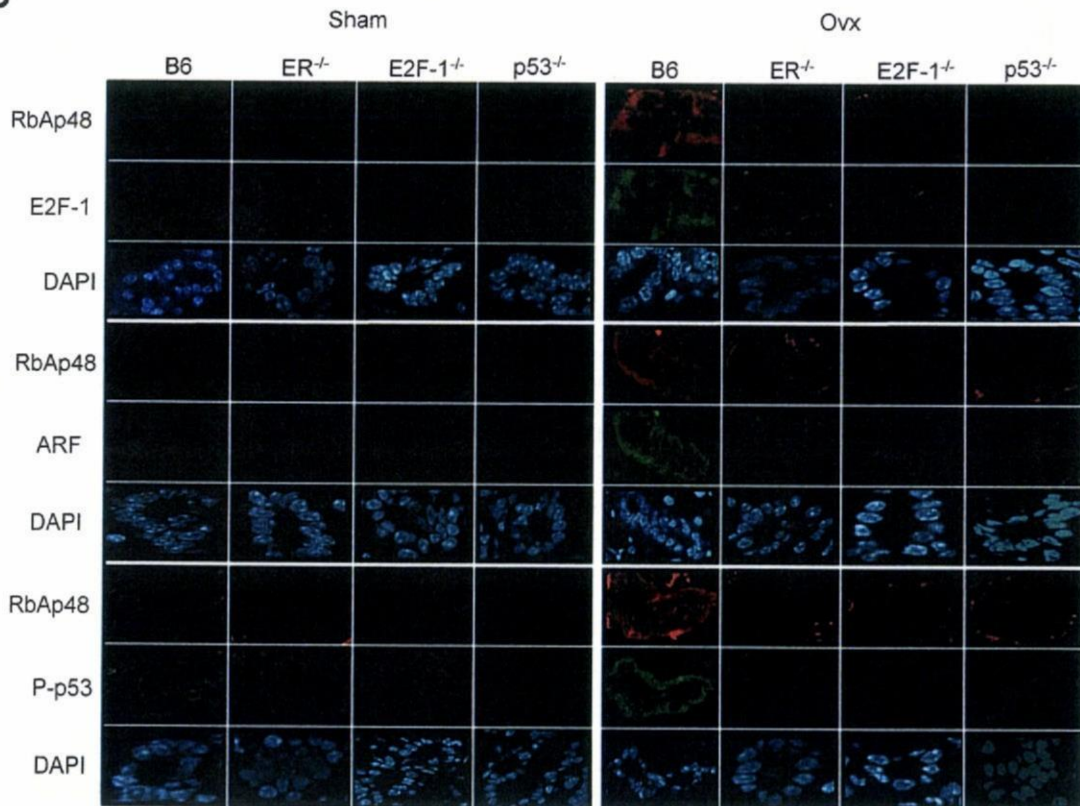
C
Sham
Ovx
B6
$ER^{-/-}$
$E2F-1^{-/-}$
$p53^{-/-}$
RbAp48
E2F-1
DAPI
ARF
P-p53

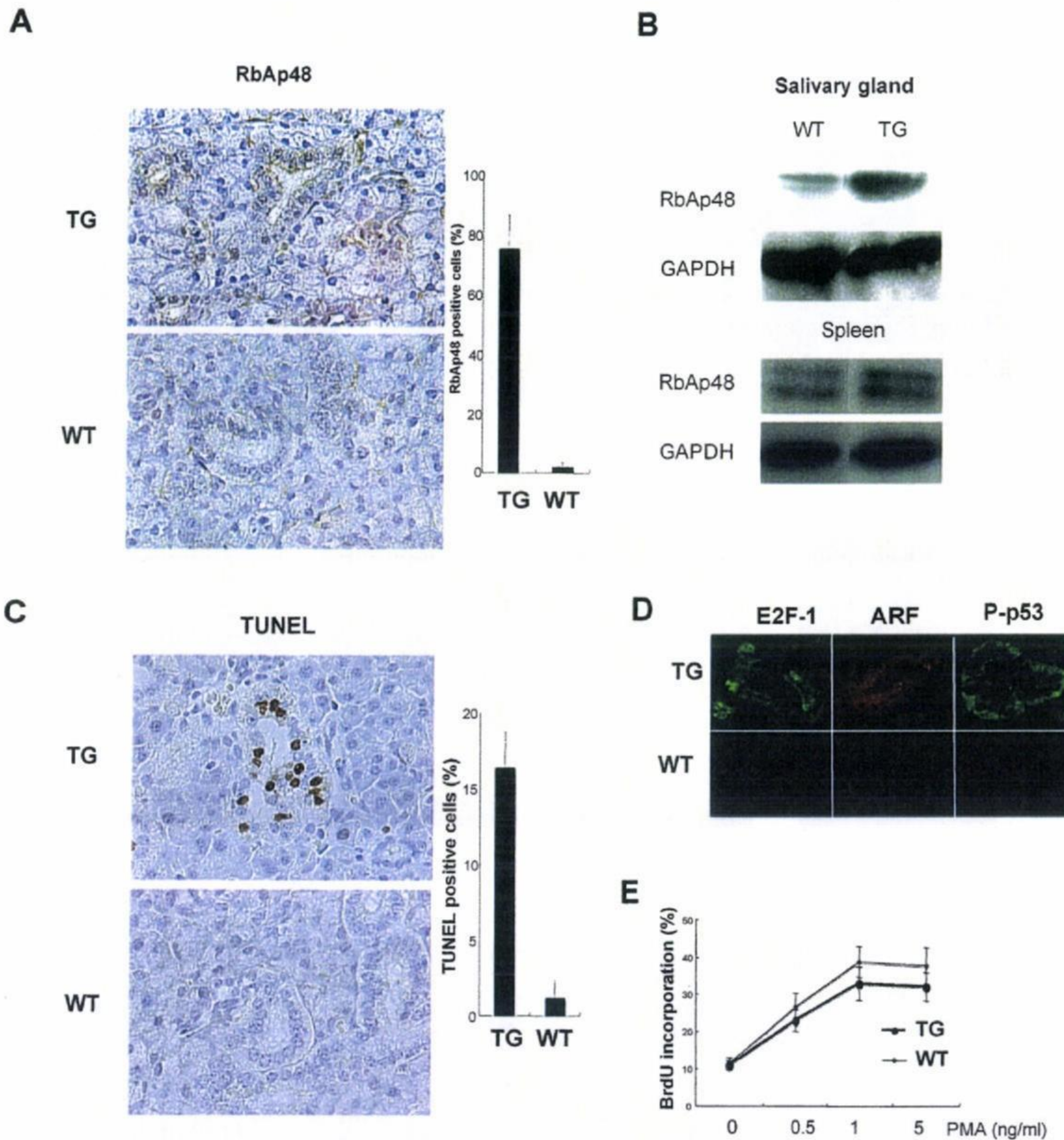

FIG. 6. RbAp48 overexpression and apoptosis in TG mice. (A) RbAp48 overexpression in the salivary gland tissues of TG mice but not WT mice at the age of 20 weeks detected by immunohistology. The percentage of RbAp48$^+$ cells was enumerated as described above (legend of Fig. 2B). (B) RbAp48 expression in the salivary gland tissues at the age of 20 weeks of TG mice compared with age-matched WT mice as detected by Western blotting. No differences in the levels of RbAp48 expression in spleens of WT and TG mice were detected. GAPDH expression was used for an internal control. (C) TUNEL$^+$ apoptotic epithelial duct cells were found in salivary glands of TG mice but not of age-matched WT mice at the age of 20 weeks. The percentage of TUNEL$^+$ cells was enumerated as described above. Images are representative of five mice. (D) Expression of E2F-1, p19ARF, and P-p53 was observed by confocal microscopy in the salivary glands of RbAp48-TG mice but not WT mice. Images are representative of five mice. (E) BrdU studies of TG mice with ectopic RbAp48 in the salivary glands demonstrated that cellular proliferation is barely affected. The graph is representative of three mice.

FIG. 5. RbAp48/E2F1/ARF-p53 pathway in the salivary glands. (A) Overexpression of RbAp48 in MSG cells from B6 mice induced E2F-1, p19ARF, and phospho-p53 (P-p53) expression, and the inhibitory effect of siRNA (15 nM) of RbAp48 was observed by confocal microscopic analysis. Cont, irrelevant siRNA control. Images are representative of three independent experiments. (B) TAM-induced apoptosis was associated with RbAp48 in MSG cells from B6 mice but not from $ER^{-/-}$, $E2F1^{-/-}$, and $p53^{-/-}$ mice as detected by confocal microscopy. Images are representative of two independent experiments. (C) Coexpression of RbAp48/E2F1, RbAp48/p19ARF, and RbAp48/p53 was detected by double-labeled confocal microscopic analysis in MSG cells of OVX B6 mice but not sham B6 mice. No differences in RbAp48/E2F1, RbAp48/p19ARF, and RbAp48/p53 expression levels were observed in MSG cells of non-OVX and OVX $ER^{-/-}$, $E2F1^{-/-}$, and $p53^{-/-}$ mice. Photos are representative of two independent experiments.

lacking many N- and C-terminal phosphorylation sites (36). These findings suggest that p53 phosphorylation is a key step in E2F-1-mediated apoptosis. The transcription factor E2F-1 functions as a key regulator for both cell cycle progression and apoptosis. E2F-2-deficient T lymphocytes exhibit enhanced T-cell receptor-stimulated proliferation and a lower activation threshold, leading to the accumulation of a population of autoreactive T lymphocytes, which appear to be responsible for causing autoimmunity in E2F-2-deficient mice (24). E2F-$1^{-/-}$ mice exhibit a defect in T lymphocyte development leading to an excess of mature T cells due to a maturation stage-specific defect in thymocyte apoptosis (8).

Our recent study suggests that antiestrogenic actions have a potent effect on the proteolysis of α-fodrin autoantigen in the salivary glands through upregulation of caspase 1 and caspase 3 activity (14). We found here a proteolysis of α-fodrin and a significant increase in caspase 3 activity in addition to the elevated caspase 1 and caspase 8 activity on RbAp48-induced apoptotic HSG cells. The fodrin α-subunit of various cells has been shown to be cleaved in association with apoptosis, in particular, due to upregulation of caspase 3 (4, 15, 48). Several reports have demonstrated that estrogen may play an inhibitory role in apoptosis in endothelial cells, breast cancer cells, cardiac myocytes, prostate cells, and neuronal cells (30, 32, 41, 43). Moreover, it has been noted that some enzymatic activities are elevated in postmenopausal women compared with normal healthy women (1, 27). Increased caspase levels seem to potentiate cell death in the presence of p53-generated signals that trigger caspase activation. Activated caspases digest many cellular proteins responsible for cell cycle regulation (e.g., Rb and Mdm2) (16), DNA damage recognition and repair [e.g., DNA-dependent protein kinase, p53, and poly(ADP-ribose) polymerase], and regulation of the cellular structure (e.g., actin, lamin, and fodrin) (44, 45). All these functional and structural protein modifications lead directly to apoptosis. Moreover, RbAp48 is found not only in histone deacetylase complexes but also in ATP-dependent remodeling complexes (9). Here we show that RbAp48 specifically activates E2F-1-mediated p53 phosphorylation in the salivary gland cells but not in many of the other types of cells examined. Thus, although the association of RbAp48 with nuclear transcriptional coactivators has not been described, there is abundant evidence that these histone binding factors interact with related classes of proteins (53, 46).

Taken together, our results demonstrate a direct molecular mechanism by which estrogen deficiency might promote p53-mediated apoptosis exclusively in exocrine gland cells through RbAp48 overexpression.

ACKNOWLEDGMENT

This work was supported in part by a Grant-in-Aid for Scientific Research (no. 17109016 and 17689049) from the Ministry of Education, Science and Culture of Japan.

REFERENCES

1. **Acarturk, F., and J. R. Robinson.** 1996. Vaginal permeability and enzymatic activity studies in normal and ovariectomized rabbits. Pharm. Res. **13:**779–783.
2. **Apostolou, I., Z. Hao, K. Rajewsky, and H. von Boehmer.** 2003. Effective destruction of Fas-deficient insulin-producing B cells in type 1 diabetes. J. Exp. Med. **198:**1103–1106.
3. **Christen, U., and M. G. Von Herrath.** 2002. Apoptosis of autoreactive CD8 lymphocytes as a potential mechanism for the abrogation of type 1 diabetes by islet-specific TNF-α expression at a time when the autoimmune process is already ongoing. Ann. N. Y. Acad. Sci. **958:**166–169.
4. **Cryns, V. L., L. Bergeron, H. Zhu, H. Li, and J. Yuan.** 1996. Specific cleavage of alpha-fodrin during Fas- and tumor necrosis factor-induced apoptosis is mediated by an interleukin-1beta-converting enzyme/Ced-3 protease distinct from the poly(ADP-ribose) polymerase protease. J. Biol. Chem. **271:**31277–31282.
5. **Ding, H. F., Y. L. Lin, G. McGill, P. Juo, H. Zhu, J. Blenis, J. Yuan, and D. E. Fisher.** 2000. Essential role for caspase-8 in transcription-independent apoptosis triggered by p53. J. Biol. Chem. **275:**38905–38911.
6. **Dou, Q. P., B. An, and P. L. Will.** 1995. Induction of a retinoblastoma phosphatase activity by anticancer drugs accompanies p53-independent G1 arrest and apoptosis. Proc. Natl. Acad. Sci. USA **92:**9019–9023.
7. **Enders, A., P. Bouillet, H. Puthalakath, Y. Xu, D. M. Tarlinton, and A. Strasser.** 2003. Loss of the proapoptotic BH3-only Bcl-2 family member Bim inhibits BCR stimulation-induced apoptosis and deletion of autoreactive B cells. J. Exp. Med. **198:**1119–1126.
8. **Field, S. J., F. Y. Tsai, F. Kuo, A. M. Zubiaga, W. G. Kaelin, Jr., D. M. Livingston, S. H. Orkin, and M. E. Greenberg.** 1996. E2F-1 functions in mice to promote apoptosis and suppress proliferation. Cell **85:**549–561.
9. **Gdula, D. A., R. Sandaltzopoulos, T. Tsukiyama, V. Ossipow, and C. Wu.** 1998. Inorganic pyrophosphatase is a component of the *Drosophila* nucleosome remodeling factor complex. Genes Dev. **12:**3206–3216.
10. **Haneji, N., T. Nakamura, K. Takio, K. Yanagi, H. Higashiyama, I. Saito, S. Noji, H. Sugino, and Y. Hayashi.** 1997. Identification of α-fodrin as a candidate autoantigen in primary Sjogren's syndrome. Science **276:**604–607.
11. **Hiebert, S. W.** 1993. Regions of the retinoblastoma gene product required for its interaction with the E2F transcription factor are necessary for E2 promoter repression and pRb-mediated growth suppression. Mol. Cell. Biol. **13:**3384–3391.
12. **Hugues, S, E. Mougneau, W. Ferlin, D. Jeske, P. Hofman, D. Homann, L. Beaudoin, C. Schrike, M. Von Herrath, A. Lehuen, and N. Glaichenhaus.** 2002. Tolerance to islet antigens and prevention from diabetes induced by limited apoptosis of pancreatic β cells. Immunity **16:**169–181.
13. **Ishimaru, N., K. Saegusa, K. Yanagi, N. Haneji, I. Saito, and Y. Hayashi.** 1999. Estrogen deficiency accelerates autoimmune exocrinopathy in murine Sjogren's syndrome through Fas-mediated apoptosis. Am. J. Pathol. **155:** 173–181.
14. **Ishimaru, N., R. Arakaki, M. Watanabe, M. Kobayashi, K. Miyazaki, and Y. Hayashi.** 2003. Development of autoimmune exocrinopathy resembling Sjogren's syndrome in estrogen deficient mice of healthy background. Am. J. Pathol. **163:**1481–1490.
15. **Janicke, R. U., M. L. Sprengart, M. R. Wati, and A. G. Porter.** 1998. Caspase-3 is required for DNA fragmentation and morphological changes associated with apoptosis. J. Biol. Chem. **273:**9357–9360.
16. **Katsuda, K., M. Kataoka, F. Uno, T. Murakami, T. Kondo, J. A. Roth, N. Tanaka, and T. Fujiwara.** 2002. Activation of caspase-3 and cleavage of Rb are associated with p16-mediated apoptosis in human non-small cell lung cancer cells. Oncogene **21:**2108–2113.
17. **Kyprianou, N., H. F. English, N. E. Davidson, and J. T. Isaacs.** 1991. Programmed cell death during regression of the MCF-7 human breast cancer following estrogen ablation. Cancer Res. **51:**162–166.
18. **Lai, A., J. M. Lee, W. M. Yang, J. A. DeCaprio, W. G. Kaelin, Jr., E. Seto, and P. E. Branton.** 1999. RBP1 recruits both histone deacetylase-dependent and -independent repression activities to retinoblastoma family proteins. Mol. Cell. Biol. **19:**6632–6641.
19. **Lamhamedi-Cherradi, S. E., S. J. Zheng, K. A. Maguschak, J. Peschon, and Y. H. Chen.** 2003. Defective thymocyte apoptosis and accelerated autoimmune diseases in TRAIL$^{-/-}$ mice. Nat. Immunol. **4:**255–260.
20. **Lieman, J. H., L. A. Worley, and J. W. Harbour.** 2005. Loss of Rb-E2F repression results in caspase-8-mediated apoptosis through inactivation of focal adhesion kinase. J. Biol. Chem. **280:**10484–10490.
21. **Marchenko, N. D., A. Zaika, and U. M. Moll.** 2000. Death signal-induced localization of p53 protein to mitochondria. A potential role in apoptotic signaling. J. Biol. Chem. **275:**16202–16212.
22. **Mikkelsen, T. R., J. Brandt, H. J. Larsen, B. B. Larsen, K. Poulsen, J. Ingerslev, N. Din, and J. P. Hjorth.** 1992. Tissue-specific expression in the salivary glands of transgenic mice. Nucleic Acids Res. **20:**2249–2255.
23. **Miyagishi, M., and K. Taira.** 2002. U6 promoter-driven siRNAs with four uridine 3′ overhangs efficiently suppress targeted gene expression in mammalian cells. Nat. Biotechnol. **20:**497–500.
24. **Murga, M., O. Fernandez-Capetillo, S. J. Field, B. Moreno, L. R. Borlado, Y. Fujiwara, D. Balomenos, A. Vicario, A. C. Carrera, S. H. Orkin, M. E. Greenberg, and A. M. Zubiaga.** 2001. Mutation of E2F2 in mice causes enhanced T lymphocyte proliferation, leading to the development of autoimmunity. Immunity **15:**959–970.
25. **Nicolas, E., S. Ait-Si-Ali, and D. Trouche.** 2001. The histone deacetylase HDAC3 targets RbAp48 to the retinoblastoma protein. Nucleic Acids Res. **29:**3131–3136.
26. **Nicolas, E., V. Morales, L. Magnaghi-Jaulin, A. Harel-Bellan, H. Richard-Foy, and D. Trouche.** 2000. RbAp48 belongs to the histone deacetylase complex

that associates with the retinoblastoma protein. J. Biol. Chem. **275:**9797–9804.

27. **Oner, P., S. Bekpinar, F. Cinar, and A. Argun.** 1994. Relationship of some endogenous sex steroid hormones to leukocyte arylsulphatase A activities in pre- and postmenopausal healthy women. Horm. Metab. Res. **26:**301–304.
28. **Oren, M.** 2003. Decision making by p53: life, death and cancer. Cell Death Differ. **10:**431–442.
29. **Paramio, J. M., C. Segrelles, M. L. Casanova, and J. L. Jorcano.** 2000. Opposite functions for E2F1 and E2F4 in human epidermal keratinocyte differentiation. J. Biol. Chem. **275:**41219–41226.
30. **Pelzer, T., M. Schumann, M. Neumann, T. de Jager, M. Stimpel, E. Serfling, and L. Neyses.** 2000. 17β-Estradiol prevents programmed cell death in cardiac myocytes. Biochem. Biophys. Res. Commun. **268:**192–200.
31. **Petrovsky, N., D. Silva, L. Socha, R. Slattery, and B. Charlton.** 2002. The role of Fas ligand in beta cell destruction in autoimmune diabetes of NOD mice. Ann. N. Y. Acad. Sci. **958:**204–208.
32. **Pike, C. J.** 1999. Estrogen modulates neuronal Bcl-xL expression and beta-amyloid-induced apoptosis: relevance to Alzheimer's disease. J. Neurochem. **72:**1552–1563.
33. **Qian, Y. W., and E. Y. Lee.** 1995. Dual retinoblastoma-binding proteins with properties related to a negative regulator of ras in yeast. J. Biol. Chem. **270:**25507–25513.
34. **Qian, Y. W., Y. C. Wang, R. E. Jr. Hollingsworth, D. Jones, N. Ling, and E. Y. Lee.** 1993. A retinoblastoma-binding protein related to a negative regulator of Ras in yeast. Nature **364:**648-652.
35. **Rathmell, J. C., and C. B. Thompson.** 2002. Pathways of apoptosis in lymphocyte development, homeostasis, and disease. Cell **109:**S97–107.
36. **Rogoff, H. A., M. T. Pickering, M. E. Debatis, S. Jones, and T. F. Kowalik.** 2002. E2F1 induces phosphorylation of p53 that is coincident with p53 accumulation and apoptosis. Mol. Cell. Biol. **22:**5308–5318.
37. **Ruuls, S. R., R. M. Hoek, V. N. Ngo, T. McNeil, L. A. Lucian, M. J. Janatpour, H. Korner, H. Scheerens, E. M. Hessel, J. G. Cyster, L. M. McEvoy, and J. D. Sedgwick.** 2001. Membrane-bound TNF supports secondary lymphoid organ structure but is subservient to secreted TNF in driving autoimmune inflammation. Immunity **15:**533–543.
38. **Saegusa, K., N. Ishimaru, K. Yanagi, K. Mishima, R. Arakaki, T. Suda, I. Saito, and Y. Hayashi.** 2002. Prevention and induction of autoimmune exocrinopathy is dependent on pathogenic autoantigen cleavage in murine Sjogen's syndrome. J. Immunol. **169:**1050–1057.
39. **Saito, I., K. Haruta, M. Shimuta, H. Inoue, H. Sakurai, K. Yamada, N. Ishimaru, H. Higashiyama, T. Sumida, H. Ishida, T. Suda, T. Noda, Y. Hayashi, and K. Tsubota.** 1999. Fas ligand-mediated exocrinopathy resembling Sjogren's syndrome in mice transgenic for IL-10. J. Immunol. **162:**2488–2494.
40. **Shirasuna, K., M. Sato, and T. Miyazaki.** 1981. A neoplastic epithelial duct cell line established form an irradiated human salivary gland. Cancer **48:**745–752.
41. **Spyridopoulos, I., A. Sullivan, M. Kearney, J. Isner, and D. Losordo.** 1997. Estrogen-receptor-mediated inhibition of human endothelial cell apoptosis. Estradiol as a survival factor. Circulation **95:**1505–1514.
42. **Stassi, G., and R. De Maria.** 2002. Autoimmune thyroid disease: new models of cell death in autoimmunity. Nat. Rev. Immunol. **2:**195–204.
43. **Szende, B., I. Romics, and L. Vass.** 1993. Apoptosis in prostate cancer after hormonal treatment. Lancet **342:**1422.
44. **Tan, X., and J. Y. J. Wang.** 1998. The caspase-RB connection in cell death. Trends Cell Biol. **8:**116–120.
45. **Vanags, D. M., M. I. Porn-Ares, S. Coppola, D. H. Burgess, and S. Orrenius.** 1996. Protease involvement in fodrin cleavage and phosphatidylserine exposure in apoptosis. J. Biol. Chem. **271:**31075–31085.
46. **Vaute, O., E. Nicolas, L. Vandel, and D. Trouche.** 2002. Functional and physical interaction between the histone methyl transferase Suv39H1 and histone deacetylases. Nucleic Acids Res. **30:**475–481.
47. **Vousden, K. H.** 2000. p53: death star. Cell **103:**691–694.
48. **Wang, K. K., R. Posmantur, R. Nath, K. McGinnis, M. Whitton, R. V. Talanian, S. B. Glantz, and J. S. Morrow.** 1998. Simultaneous degradation of αII- and βII-spectrin by caspase 3 (CPP32) in apoptotic cells. J. Biol. Chem. **273:**22490–22497.
49. **Wang, R. H., C. W. Liu, V. L. Avramis, and N. Berndt.** 2001. Protein phosphatase 1α-mediated stimulation of apoptosis is associated with dephosphorylation of the retinoblastoma protein. Oncogene **20:**6111–6122.
50. **Whitacre, C. C.** 2001. Sex differences in autoimmune disease. Nat. Immunol. **2:**777–780.
51. **Whitacre, C. C., S. C. Reingold, and P. A. O'Looney.** 1999. A gender gap in autoimmunity. Science **283:**1277–1278.
52. **Yu, J. Y., S. L. DeRuiter, and D. L. Turner.** 2002. RNA interference by expression of short-interfering RNAs and hairpin RNAs in mammalian cells. Proc. Natl. Acad. Sci. USA **99:**6047–6052.
53. **Zhang, Q., N. Vo, and R. H. Goodman.** 2000. Histone binding protein RbAp48 interacts with a complex of CREB binding protein and phosphorylated CREB. Mol. Cell. Biol. **20:**4970–4978.
54. **Zhang, Y., B. O'Brien, J. Trudeau, R. Tan, P. Santamaria, and J. P. Dutz.** 2002. In situ β cell death promotes priming of diabetogenic CD8 T lymphocytes. J. Immunol. **168:**1466–1472.

Immunity 24, 165–177, February 2006 ©2006 Elsevier Inc. DOI 10.1016/j.immuni.2005.12.011

CCR7-Dependent Cortex-to-Medulla Migration of Positively Selected Thymocytes Is Essential for Establishing Central Tolerance

Hirotsugu Kurobe,[1,2] Cunlan Liu,[1] Tomoo Ueno,[1,5] Fumi Saito,[1] Izumi Ohigashi,[1] Natalie Seach,[5] Rieko Arakaki,[3] Yoshio Hayashi,[3] Tetsuya Kitagawa,[2] Martin Lipp,[4] Richard L. Boyd,[5] and Yousuke Takahama[1,*]
[1] Division of Experimental Immunology
Institute for Genome Research
University of Tokushima
Tokushima 770-8503
Japan
[2] Department of Cardiovascular Surgery
[3] Department of Oral Molecular Pathology
Institute of Health Biosciences
University of Tokushima
Tokushima 770-8503
Japan
[4] Department of Molecular Tumorgenetics
and Immunogenetics
Max-Delbrück Center for Molecular Medicine
Berlin 13125
Germany
[5] Monash Immunology and Stem Cell Laboratories
Monash University
Clayton 3800
Victoria
Australia

Summary

Immature CD4$^+$CD8$^+$ thymocytes, which are generated in the thymic cortex, are induced upon positive selection to differentiate into mature T lymphocytes and relocate to the thymic medulla. It was recently shown that a chemokine signal via CCR7 is essential for the cortex-to-medulla migration of positively selected thymocytes in the thymus. However, the role of the cortex-to-medulla migration in T cell development and selection has remained unclear. The present study shows that the developmental kinetics and the thymic export of mature thymocytes were undisturbed in adult mice lacking CCR7 or its ligands (CCR7L). The inhibition of sphingosine-1-phosphate-mediated lymphocyte egress from the thymus led to the accumulation of mature thymocytes in the cortex of CCR7- or CCR7L-deficient mice, unlike the accumulation in the medulla of normal mice, thereby suggesting that mature thymocytes may be exported directly from the cortex in the absence of CCR7 signals. However, the thymocytes that were generated in the absence of CCR7 or CCR7L were potent in causing autoimmune dacryoadenitis and sialadenitis in mice and were thus incapable of establishing central tolerance to organ-specific antigens. These results indicate that CCR7-mediated cortex-to-medulla migration of thymocytes is essential for establishing central tolerance rather than for supporting the maturation or export of thymocytes.

*Correspondence: takahama@genome.tokushima-u.ac.jp

Introduction

The thymus is an organ that supports the differentiation and selection of T lymphocytes (Miller, 1961; Ritter and Boyd, 1993; Anderson and Jenkinson, 2001). Lymphoid progenitor cells enter the thymus via the surrounding mesenchymal layer before vascularization during fetal development (Bleul and Boehm, 2000) and via blood vessels that are enriched at the cortico-medulla junction in adulthood (Lind et al., 2001). Several chemokines have been suggested to play a crucial role in the positioning of T precursor cells to the subcapsular zone of the outer cortex of the thymus (Plotkin et al., 2003; Misslitz et al., 2004; Benz et al., 2004; Gray et al., 2005; Liu et al., 2005), where immature CD4$^+$CD8$^+$ double-positive (DP) thymocytes are newly generated (Ritter and Boyd, 1993; Takahama et al., 1994). The DP thymocytes crawl through the cortical environment, seeking to encounter the self-MHC-peptide complex expressed by various stromal cells in the cortex, including the cortical thymic epithelial cells (cTEC) (Bousso et al., 2002). Upon TCR engagement by the MHC-peptide ligands, the DP thymocytes stop crawling and initiate the signaling processes for positive and negative selection, which result in further differentiation into CD4$^+$CD8$^-$/CD4$^-$CD8$^+$ single-positive (SP) thymocytes and apoptotic deletion, respectively (Bousso et al., 2002; Palmer, 2003). Concurrently to the differentiation into SP thymocytes, positively selected thymocytes are relocated to the medulla (Ritter and Boyd, 1993; van Ewijk et al., 1994; Witt et al., 2005). The newly generated SP thymocytes are semimature, being functionally incompetent and susceptible to various apoptotic signals including dexamethasone, and undergo further maturation to become mature SP thymocytes that are functional, dexamethasone-resistant, and CD62L^{high}CD69^{low} (Reichert et al., 1986a; Ramsdell et al., 1991; Kishimoto and Sprent, 1997; Gabor et al., 1997; Sheard et al., 2004). The mature SP thymocytes are exported from the thymus via chemotaxis toward sphingosine-1-phosphate (S1P) in the circulation and are systemically distributed as functional yet naive T lymphocytes (Matloubian et al., 2004; Allende et al., 2004). The maturation of SP thymocytes is thought to occur within the medulla (Egerton et al., 1990; Scollay and Godfrey, 1995), and the export to the circulation is thought to occur through the perivascular space in the medulla (Ushiki, 1986; Kato, 1997).

In the thymic medulla, medullary thymic epithelial cells (mTEC) specifically express the nuclear protein AIRE, which is essential for the promiscuous expression of organ-specific self-antigens by mTEC (Zuklys et al., 2000; Gotter and Kyewski, 2004). AIRE deficiency results in autoimmune-polyendocrinopathy-candidiasis ectodermal dystrophy (APECED) in human (Nagamine et al., 1997; Aaltonen et al., 1997) and mouse (Anderson et al., 2002; Liston et al., 2003; Kuroda et al., 2005). Thus, AIRE expressed by mTEC is essential for establishing the central tolerance of T lymphocytes to organ-specific antigens. The molecular mechanisms involved in the differentiation of thymic epithelial progenitor cells into

AIRE-expressing mTEC have remained vague (Blackburn et al., 2002; Farr et al., 2002), although recent analyses have shown that similar to the organogenesis of lymph nodes and Peyer's patches, the NFκB-mediated signals via LTβR, TRAF6, NIK, and relB are critical for the development of the thymic medulla that regulates central tolerance (Burkly et al., 1995; Boehm et al., 2003; Kajiura et al., 2004; Akiyama et al., 2005). It has also been suggested that the thymic medulla contributes to central tolerance by dendritic cells (DCs), which are of hematopoietic origin and are predominantly localized within the thymic medulla (Flotte et al., 1983; Fairchild and Austyn, 1990). The average lifespan of the newly generated SP thymocytes in the thymus is 12 days (Egerton et al., 1990; Scollay and Godfrey, 1995). During this period, the thymic medulla is thought to provide an environment in which the SP thymocytes are induced to mature and are tuned to acquire central tolerance. However, whether the medulla migration of positively selected thymocytes is essential for the maturation of SP thymocytes, for the acquisition of central tolerance, or for the export from the thymus is unclear.

Previous studies with the chemotaxis assay and mRNA measurement showed that CCR7 expression by developing thymocytes is associated with the phenotypic stage of cortex-to-medulla migration, during the development of immature DP thymocytes to mature SP thymocytes (Kim et al., 1998; Campbell et al., 1999). We have recently shown that CCR7 ligands (CCR7L species CCL19 and CCL21) in the thymus are predominantly produced by mTEC and are localized in the medulla, whereas TCR engagement of immature cortical DP thymocytes elevates the cell surface expression of CCR7 (Ueno et al., 2002, 2004). In mice deficient in CCR7 or CCR7L, the mature SP thymocytes are arrested in the cortex and do not accumulate in the medulla (Ueno et al., 2004). These results indicate that the CCR7 signals are essential for the migration of positively selected thymocytes from the cortex to the medulla. By using mice that are deficient in CCR7 or CCR7L, the present study addresses whether T cells may be exported from the thymic cortex without accumulation in the medulla and whether central tolerance to organ-specific self-antigens may be affected by the absence of medulla migration. We show that the pharmacological inhibition of S1P-mediated thymocyte egress in CCR7- or CCR7L-deficient mice results in the accumulation of mature thymocytes in the cortex, suggesting that mature thymocytes may be exported via the S1P-dependent mechanism from the cortex in the absence of CCR7 signals. We also show that in the absence of CCR7-dependent medulla migration, mature thymocytes are incapable of acquiring tolerance to lacrimal and salivary glands and are potent in inducing autoimmune exocrinopathy similar to Sjögren's syndrome.

Results

S1P Blockade Induces Accumulation of Mature Thymocytes in the Thymic Cortex of CCR7- or CCR7L-Deficient Mice

We have previously shown that mice deficient in CCR7 or CCR7L were defective in the cortex-to-medulla migration of thymocytes and that SP thymocytes generated in CCR7L-deficient (*plt/plt*, P/P) or CCR7-deficient (7/7) mice were barely accumulated in the thymic medulla (Ueno et al., 2004). SP thymocytes in these mutant mice appeared normal in terms of frequency and underwent maturation, including TCR responsiveness and formation of surface phenotypes such as CD62L and CD69 (Ueno et al., 2004). In vivo 5-bromo-2-deoxyuridine (BrdU) labeling showed that SP thymocytes and DP thymocytes in these mutant mice were normally generated according to the developmental kinetics (Figure 1A). In addition, intrathymic FITC administration showed that SP thymocytes in CCR7L- or CCR7-deficient mice were normally exported from the adult thymus to the circulation (Ueno et al., 2004). These results indicate that in CCR7L- or CCR7-deficient adult mice, SP thymocytes show normal maturation without medulla accumulation and normal export from the thymus.

The above results suggested the possibility that the mature SP thymocytes generated in CCR7- or CCR7L-deficient mice might be exported from the cortex without migrating into the medulla. In order to examine this possibility, the mice were administered FTY720, an immunosuppressive compound that is phosphorylated in vivo by sphingosine kinases and acts as an S1P mimetic to sequester T lymphocytes in the thymus and lymph nodes (Chiba et al., 1998; Brinkmann et al., 2002). It was previously shown that S1P1, one of the S1P receptors, is expressed by mature SP thymocytes and that S1P1 is required for the egress of T lymphocytes from the thymus and lymph nodes (Matloubian et al., 2004; Allende et al., 2004). Among the thymocyte subpopulations, S1P1 mRNA was highly expressed in SP thymocytes rather than DP or double-negative (DN) thymocytes (Matloubian et al., 2004; Allende et al., 2004; also shown in Figure 1B). Within the SP thymocytes, the S1P1 expression was predominantly detected in the $CD62L^{high}CD69^{low}$ mature subpopulation rather than the $CD62L^{low}CD69^{high}$ semimature subpopulation (Matloubian et al., 2004; also shown in Figure 1B). Similar to S1P1 expression, CCR7 expression was much higher in SP thymocytes than in DP or DN thymocytes (Kwan and Killeen, 2004; Misslitz et al., 2004; also shown in Figure 1B). Unlike S1P1 expression, however, CCR7 expression was detected in $CD62L^{low}CD69^{high}$ semimature thymocytes as well as in $CD62L^{high}CD69^{low}$ mature thymocytes (Figure 1B). The CCR7 mRNA expression levels measured by quantitative RT-PCR analysis agreed with the CCR7 surface expression levels measured by flow cytometry analysis with CCL19-Ig fusion protein (Figures 1C and 1D). $CCR7^{high}TCR\beta^{high}$ thymocytes contained both the $CD62L^{low}CD69^{high}$ semimature compartment and the $CD62L^{high}CD69^{low}$ mature compartment, whereas $CCR7^{negative/low}TCR\beta^{high}$ thymocytes predominantly contained the $CD62L^{low}CD69^{high}$ semimature compartment (Figure 1C). CCR7 expression was higher in $CD62L^{high}CD69^{low}$ mature thymocytes than in $CD62L^{low}CD69^{high}$ semimature thymocytes (Figure 1D). These results indicate that CCR7 expression is detected in both $CD62L^{low}CD69^{high}$ semimature and $CD62L^{high}CD69^{low}$ mature thymocytes, whereas S1P1 expression is detected predominantly in the $CD62L^{high}CD69^{low}$ mature subpopulation,

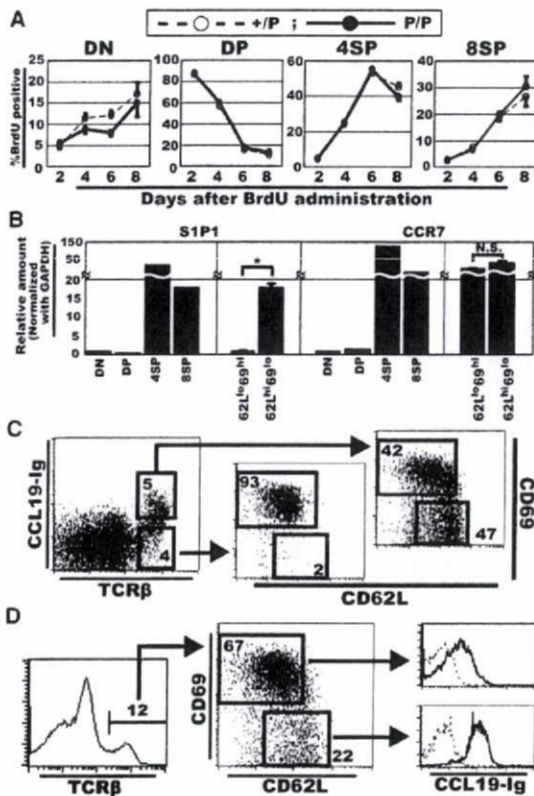

Figure 1. Expression and Function of CCR7 in Thymocyte Subpopulations

(A) Kinetics of mature thymocytes in mice deficient in CCR7L (*plt/plt*, P/P) and their heterozygous control mice (+/P). Thymocytes from BrdU-treated adult mice were stained for CD4, CD8, and BrdU. Plots show means and standard deviations (symbols and bars, respectively; the number of mice used for individual plots ranged from five to seven) of the frequency of BrdU-positive cells within the indicated CD4/CD8 populations of thymocytes on the indicated day of analysis. All the data sets between +/P and P/P groups were not significantly different at all the indicated days of analysis in all of the indicated thymocyte subpopulations (including the data on DN thymocytes) by the Student's t test.

(B) Adult thymocytes from B6 mice were two-color stained for CD4 and CD8 and sorted for DN, DP, CD4SP, and CD8SP populations. Adult B6 thymocytes were also three-color stained for TCRβ, CD62L, and CD69 and were sorted for TCRβ^{high}CD62L^{low}CD69^{high} semimature and TCRβ^{high}CD62L^{high}CD69^{low} mature subpopulations. Purity was >97% for CD4/CD8 two-color-sorted fractions and >87% for TCRβ/CD62L/CD69 three-color-sorted fractions. Relative mRNA levels (means and standard errors; n = 3) obtained by quantitative RT-PCR for S1P1 and CCR7, which were normalized to GAPDH mRNA levels, are shown. Asterisk indicates $p < 0.05$ by the Student's t test. N.S., not significant.

(C and D) Adult B6 thymocytes were examined for CCR7 surface expression by using CCL19-Ig, which specifically detects CCR7 on the cell surface. Cells were also stained with PE-labeled anti-TCRβ antibody, FITC-labeled anti-CD62L antibody, and PE-Cy5-labeled anti-CD69 antibody. Where indicated, data were gated for TCRβ^{high}CCR7^{high} and TCRβ^{high}CCR7$^{negative/low}$ cells (C) and TCRβ^{high}CD62L^{low}CD69^{high} and TCRβ^{high}CD62L^{high}CD69^{low} cells (D). Numbers indicate frequencies of cells within the indicated boxes. Dotted lines indicate control staining profiles without CCL19-Ig. Shown are representative results of four independent measurements.

suggesting that the CCR7-mediated medulla migration and the S1P1-mediated thymocyte egress are differently and sequentially regulated during SP thymocyte maturation.

Importantly, FTY720 treatment induced the accumulation of SP thymocytes in CCR7- or CCR7L-deficient mice as well as in normal mice (Figures 2A and 2B). Among the SP thymocytes, the accumulation was specifically induced in the CD62L^{high}CD69^{low} mature population, in either the CD4SP or the CD8SP compartment (Figures 2A and 2C). Thus, the FTY720-mediated S1P blockade of thymocyte egress to the circulation results in the accumulation of CD62L^{high} mature SP thymocytes even in CCR7- or CCR7L-deficient mice, in which most SP thymocytes are arrested in the cortex and are defective in migrating into the medulla.

It was therefore interesting to identify the location in the thymus where mature thymocytes were accumulating upon FTY720 treatment in CCR7- or CCR7L-deficient mice, as the location for this accumulation would correspond to the microenvironment where S1P would otherwise act to attract mature thymocytes into the circulation. To this end, thymus sections from FTY720-treated mice were stained with mature-thymocyte-specific anti-CD62L antibody and either mTEC-specific ER-TR5 or cTEC-specific ER-TR4 monoclonal antibodies (Figure 3). In agreement with the increase in the CD62L^{high} SP thymocyte population as determined by flow cytometry analysis (Figure 2C), the FTY720 treatment markedly increased the CD62L^{high} thymocyte population in normal mice as well as in CCR7- or CCR7L-deficient mice (Figure 3A). In a parallel analysis of the sections, the increased CD62L^{high} cells were indeed shown to belong to CD4 or CD8 single-positive thymocytes in normal and mutant mice (data not shown), indicating that the CD62L^{high} thymocytes increased in Figure 3A represented mature SP thymocytes. Most remarkably, the FTY720-mediated accumulation of CD62L^{high} mature thymocytes was predominantly detected in the cortex and not the medulla of CCR7- or CCR7L-deficient mice, whereas the CD62L^{high} mature thymocytes were accumulated predominantly in the medulla of control mice (Figure 3A). In the cortex of FTY720-mediated CCR7- or CCR7L-deficient mice and in the medulla of FTY720-mediated control mice, the analysis at higher magnification detected areas where CD62L^{high} thymocytes accumulated around CD31^{+} endothelial vessels (Figure 3B). In some of those areas, CD62L^{high} thymocytes were found even within the perivascular space surrounded by CD31^{+} endothelial and ER-TR7^{+} mesenchymal cells (Figure 3C). In contrast, no or very few CD62L^{high} thymocytes were found in the medulla of FTY720-treated CCR7- or CCR7L-deficient mice and in the cortex of FTY720-treated control mice (Figures 3A, 3B, and 3C). These results indicate that upon FTY720 treatment, the mature SP thymocytes in CCR7- or CCR7L-deficient mice are accumulated in the cortex rather than the medulla of the thymus and are found even in the cortical perivascular space, suggesting the possibility that mature thymocytes generated in CCR7- or CCR7L-deficient mice may be exported from the cortex through the cortical perivascular space in a S1P-dependent manner.

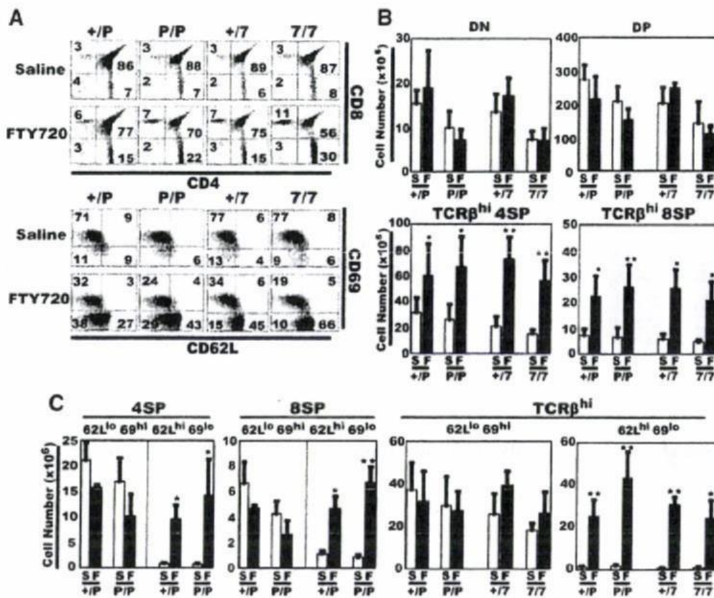

Figure 2. Accumulation of Mature Thymocytes by FTY720-Mediated S1P Blockade

Flow cytometry analysis of thymocytes from CCR7L-deficient mice (*plt/plt*, P/P), CCR7-deficient mice (7/7), and their heterozygous control mice (+/P and +/7), which were treated with either saline (S) or FTY720 (F). The profiles of CD62L and CD69 in (A) were gated for TCRβ^{high} cells. Numbers in (A) indicate frequencies of cells within the quadrants.

(B and C) Means and standard errors (the numbers of mice analyzed ranged from four to 11 in [B] and three to six in [C]) of the absolute numbers of indicated thymocyte subpopulations are shown. Asterisk indicates $p < 0.05$ and double asterisk indicates $p < 0.005$ by the Student's t test.

Intrathymic Localization of AIRE$^+$ Epithelial Cells and Dendritic Cells in CCR7- or CCR7L-Deficient Mice

We then addressed whether thymic function in inducing central tolerance is affected in CCR7- or CCR7L-deficient mice. It was previously reported that the thymic medulla contributes to establishing central tolerance by AIRE-expressing mTEC (Zuklys et al., 2000; Anderson et al., 2002; Liston et al., 2003; Kuroda et al., 2005) and medulla-localized DCs (Fairchild and Austyn, 1990; Moore et al., 1994). We thus examined whether AIRE$^+$ mTEC and CD11c$^+$ DCs were indeed localized within the medulla in CCR7- or CCR7L-deficient mice. Figure 4 shows that AIRE$^+$ cells in the thymus were predominantly confined in the medullary region in CCR7- or CCR7L-deficient mice as well as in normal mice (Figures 4A and 4B). The analysis at high magnification showed that in the thymus of CCR7- or CCR7L-deficient mice as well as in normal mice, AIRE expression was found in the nuclei, as previously reported (Bjorses et al., 1999; Rinderle et al., 1999), and in a fraction of keratin$^+$MTS-10$^+$ mTEC (Figure 4C). It was also shown that in CCR7- or CCR7L-deficient mice, as in normal mice, CD11c$^+$ DCs were predominantly localized in the medulla, although some CD11c$^+$ DCs were sparsely found in the cortex even in normal mice (Figures 4D and 4E). These results indicate that similar to that of normal mice, AIRE in the thymus of CCR7- or CCR7L-deficient mice are predominantly expressed in the medulla by a fraction of mTEC. The results also show that DCs in the thymus are enriched in the medulla in CCR7- or CCR7L-deficient mice, indicating that CCR7 signals are not required for the accumulation of DCs in the thymic medulla. The results suggest that developing thymocytes in CCR7- or CCR7L-deficient mice, which are not accumulated in the medulla, may fail to directly interact with AIRE$^+$ mTEC.

Thymocytes Generated in CCR7L-Deficient Mice Are Potent in Inducing Autoimmune Exocrinopathy

The above results raised the possibility that the establishment of thymic-medulla-dependent central tolerance to organ-specific antigens might be affected in CCR7- or CCR7L-deficient mice. We thus examined various organs of these mutant mice for lesions that might be associated with defective self-tolerance. As shown in Figure 5, we found that the lacrimal glands, the parotid glands, and the submandibular glands exhibited periductal lymphocyte infiltration in CCR7- or CCR7L-deficient mice (Figures 5A, 5B, and 5C). Lymphocyte infiltration in the lacrimal glands was accompanied by severe tissue damage, including the destruction of acinar cells (Figures 5A and 5D and Figure 6A). In mice up to 25 weeks old, the tissue damage was largely specific for these exocrine glands, as no apparent lesions were detected in other organs, including the trachea, thyroid, liver, spleen, kidney, intestine, adrenal gland, and ovary (data not shown). The lesions in these exocrine glands were detected in all the tested mutant mice (n = 14 for *plt/plt* mice; n = 5 for CCR7-deficient mice), even as early as 5 weeks old (Figure 5D), and were found similarly in CCR7L-deficient mice of BALB/c background as well as C57BL/6 background (Figures 5A, 5B, and 5C). The infiltrated lymphocytes were mostly CD4$^+$ T cells and B cells, and tissue-reactive antibodies were markedly deposited in the damaged tissues (Figures 6B and 6C). These results indicate that CCR7- or CCR7L-deficient mice exhibit autoimmune exocrinopathy resembling Sjögren's syndrome.

To examine whether the autoimmune exocrinopathy is a direct consequence of the defect in thymocytes, the CCR7L-deficient *plt/plt* thymocytes were transferred into RAG2-deficient mice that lacked T cells and B cells. Under this experimental condition, the *plt/plt*

thymocytes were not defective in CCR7 expression, and the host RAG2-deficient mice were not defective in CCR7L expression. CCR7-expressing *plt/plt*-derived T cells would normally migrate to CCR7L-expressing host tissues, including lymph nodes and exocrine glands, in the RAG2-deficient mice. Thus, the defect in CCR7/CCR7L signaling in this cell transfer experiment would be limited to the period of thymocyte development before the cell transfer, and the transferred thymocyte-derived T cells would exhibit no or little aberrancy in the peripheral distribution after the cell transfer. As shown in Figures 7A and 7B, the transfer of CCR7L-deficient *plt/plt* thymocytes as well as *plt/plt* spleen cells caused significant lymphocyte infiltration in the lacrimal and salivary glands. By contrast, the transfer of control *+/plt* thymocytes or *+/plt* spleen cells did not cause such lymphocyte infiltration (Figures 7A and 7B). These results indicate that the thymocytes generated without CCR7L are potent in inducing autoimmune exocrinopathy in mice and, thus, are defective in establishing central tolerance.

It was previously shown that *plt/plt* or CCR7-deficient mice are defective in forming the medullary architecture characterized by clusters of UEA-1$^+$ cells (Ueno et al., 2004). We finally addressed whether the defective central tolerance in the thymus lacking CCR7 or CCR7L is due to defective thymocyte accumulation in the medulla or defective architecture of the medullary stroma. To this end, we generated mixed bone marrow chimeras reconstituted with equal numbers of bone marrow cells from CCR7-deficient mice and normal mice and examined whether these mixed bone marrow chimeras might exhibit the autoimmune exocrinopathy. Due to the presence of normal bone-marrow-derived thymocytes, it was presumed that the medullary architecture in the mixed bone marrow chimeras would appear normal even in the presence of CCR7-deficient thymocytes. Indeed, normal architecture of the medullary region containing the UEA-1$^+$ clusters was detected in the mixed bone marrow chimeras, which was similar to that in the normal bone marrow chimeras and different from that in CCR7-deficient bone marrow chimeras (Figure 7C), whereas the accumulation of CD45.2$^+$ CCR7-deficient thymocytes in the medulla was severely defective in the mixed bone marrow chimeras (Figure 7D). However, these mixed bone marrow chimeras exhibited the autoimmune phenotypes in the lacrimal glands, including lymphocyte infiltration and tissue damage, similar to the bone marrow chimeras reconstituted with CCR7-deficient bone marrow cells alone (Figures 7E and 7F). These results indicate that CCR7-deficient bone-marrow-derived cells that are reconstituted in the normal thymus architecture are potent in inducing autoimmune exocrinopathy, suggesting that the autoimmune phenotype in CCR7-deficient mice is likely due to the lack of thymocyte accumulation in the medulla rather than the defective development of the medullary architecture. These results also indicate that CCR7-deficient bone-marrow-derived cells that are reconstituted in the presence of normally developing hematopoietic cells are still potent in inducing autoimmune exocrinopathy, suggesting that the autoimmunity in these mutant mice may be caused even in the presence of normally generated immune cells, including regulatory T cells.

Discussion

The present results show that mature thymocytes are normally generated in developmental kinetics and are normally exported in CCR7- or CCR7L-deficient adult mice. The pharmacological inhibition of S1P-mediated thymocyte egress shows that in the absence of CCR7 signals, the mature thymocytes are accumulated in the thymic cortex rather than the thymic medulla, suggesting that the S1P-mediated thymocyte egress may occur in the thymic cortex of these mutant mice. These results argue the possibility that the thymic medulla may not be required for the maturation or export of thymocytes. On the other hand, our results also show that in the absence of CCR7 signals, the mature thymocytes are incapable of acquiring tolerance to lacrimal and salivary glands and are potent in inducing autoimmune exocrinopathy. Thus, CCR7-mediated cortex-to-medulla migration of positively selected thymocytes is essential for establishing central tolerance rather than for supporting the maturation or export of thymocytes.

The Cortex and Thymocyte Export

Our results show that the developmental kinetics and the thymic export of SP thymocytes are undisturbed in adult mice lacking CCR7 or CCR7L. FTY720 treatment shows that the mature thymocytes are accumulated in the thymic cortex of CCR7- or CCR7L-deficient mice, unlike the accumulation in the medulla of normal mice. FTY720-sensitive S1P-dependent chemotaxis is essential for the egress of mature thymocytes to the circulation (Matloubian et al., 2004). Thus, the present results suggest that the mature thymocytes generated in CCR7- or CCR7L-deficient mice may be exported from the cortex without migrating into the medulla. It has been generally thought that the medulla is a place for the maturation and export of thymocytes (Ritter and Boyd, 1993; Scollay and Godfrey, 1995; Anderson and Jenkinson, 2001). Indeed, our results from the FTY720 treatment of normal mice agree with the notion that S1P-dependent thymocyte export occurs in the medulla of normal mice (Figure 3). However, our results also suggest the possibility that in the case that the positively selected thymocytes remain in the cortex without being attracted to CCR7L expressed in the medulla, the thymic cortex can not only nurture the maturation of SP thymocytes but also export the mature thymocytes. Based on these results, we propose the possibility that the thymic cortex may have the capability of fully supporting the development of T cells, including SP thymocyte maturation and the export of mature T cells. This possibility is consistent with previous findings that T cell maturation and peripheral supply are not perturbed in relB-deficient mice that lack the thymic medulla (Burkly et al., 1995).

It should be noted that we detected a minor fraction of mature SP thymocytes in the medullary areas of CCR7- or CCR7L-deficient mice (Ueno et al., 2004). However, FTY720 treatment does not cause the accumulation of mature thymocytes in the medulla of CCR7- or CCR7L-deficient mice (Figure 3), arguing the possibility that those medullary thymocytes in CCR7- or CCR7L-deficient mice do not represent mature thymocytes whose S1P-dependent egress from the thymus is blocked. It is even unclear whether those medullary thymocytes in